Physics – Uspekhi **63** (10) 975 – 993 (2020)

REVIEWS OF TOPICAL PROBLEMS PACS numbers: **73.21.–b**, **73.22.–f**, 73.43.Lp, 78.70.Gq

Collective plasma excitations in two-dimensional electron systems

V M Muravev, I V Kukushkin

DOI: https://doi.org/10.3367/UFNe.2019.07.038637

Contents

Abstract. The latest results on the study of collective plasma excitations in two-dimensional electron systems based on AlGaAs/GaAs, AlGaAs/AlAs, and MgZnO/ZnO nanostructures and graphene are considered. Special attention is paid to the interaction of two-dimensional plasma with light. The results of experimental work on the discovery of a new family of plasma oscillations are presented. Possible avenues for the further development of experiment and theory are discussed.

Keywords: plasmon, cyclotron resonance, two-dimensional electron system, nanostructure

1. Introduction

When studying a solid, we are always dealing with a system of many interacting particles. To date, there are no approaches to an exact solution to this many-body problem. Therefore, approximate models are to be used in constructing a theory. The use of approximate models is one of the attractive features of solid-state physics. Due to the relative simplicity of experimental verification of ideas, solid-state physics is a unique site for testing new concepts and approaches. One of the most fruitful ideas of solid-state physics is the concept of elementary excitations [1]. The complex correlated motion of many particles in a solid appears to be describable in terms of elementary excitations (quasiparticles) weakly interacting with each other.

Elementary excitations are divided into single-particle and collective. First, a number of quantum mechanical operations are performed in the theory: the gas of single-particle elementary excitations (quasiparticles), referred to as 'electrons' with a complex dispersion law reflecting the crystal lattice symmetry, is introduced. Then, due to Coulomb interactions, collective oscillations of electron density, so-called plasma oscillations, arise in the system of interacting electrons [2–5]. A quantum of plasma oscillations is called a plasmon. In the large wavelength limit, the frequency of these oscillations is equal to the plasma frequency

$$\omega_{\mathrm{p}} = \sqrt{\frac{4\pi n e^2}{m^*}}\,, \tag{1}$$

where n is the concentration of electrons, and m^* is the electron effective mass. Plasma excitations in a three-dimensional plasma possess weak quadratic dispersion. They are analogous to the oscillations in the classical gas discharge studied by Langmuir and Tonks [6]. It should also be noted that plasma oscillations cannot exist in a system of noninteracting electrons.

The concept of elementary excitations successfully applies to the description of two-dimensional (2D) multielectron systems on surfaces of liquid helium, silicon-based metal–dielectric–semiconductor (MDS) structures, semiconductor heterostructures with quantum wells, and new layered materials of the graphene family. The two-dimensional properties of electrons in most of these materials are ensured by the fact that the energy related to the transverse quantization exceeds all other characteristic energies (thermal energy and Fermi energy). The properties of two-dimensional plasma excitations were first described theoretically

V M Muravev, I V Kukushkin
Institute of Solid State Physics, Russian Academy of Sciences,
ul. Akademika Osip'yana 2, 142432 Chernogolovka, Moscow region, Russian Federation
E-mail: muravev@issp.ac.ru, kukush@issp.ac.ru

Received 2 July 2019, revised 23 July 2019
Uspekhi Fizicheskikh Nauk **190** (10) 1041 – 1061 (2020)
Translated by V L Derbov

in [7] in 1967. 2D plasmons were first discovered in the system of electrons on the surface of liquid helium [8] and a year later in silicon-based metal–oxide–semiconductor (MOS) split-gate transistors [9, 10]. The spectrum of plasma excitations of a 2D electron system (2DES) is described by the following expression:

$$q^2 = \varepsilon\,\frac{\omega^2}{c^2} + \left(\frac{\omega^2}{2\pi n_s e^2/m^*\varepsilon}\right)^2, \qquad \omega \gg v_0 q\,, \tag{2}$$

where n_s is the surface concentration of 2D electrons, v_0 is the Fermi velocity, and $\varepsilon(q)$ is the effective permittivity of the medium surrounding the 2DES. The second term on the right-hand side of Eqn (2) is responsible for electron–electron Coulomb correlations, while the first term describes the retarded transmission of these correlations. In the long-wavelength limit, when the retardation can be disregarded (electrostatic approximation), we arrive at the square-root gapless dispersion law for two-dimensional plasmons:

$$\omega_p = \sqrt{\frac{2\pi n_s e^2}{m^*\varepsilon}\,q}\,. \tag{3}$$

The condition for resonant excitation of 2D plasmons is $\omega_p\tau \gg 1$, where τ is the energy relaxation time of two-dimensional electrons [11, 12]. Note that this time can differ by more than two orders of magnitude from the transport relaxation time of charge carriers, measured in the same structure.

In the limit of small wave vectors, $q \ll 2\pi n_s e^2/m^* c^2$, the main role is played by electrodynamic effects, and the dispersion law (2) takes the form characteristic of a light wave propagating in a medium with the refractive index $\sqrt{\varepsilon}$: $\omega = cq/\sqrt{\varepsilon}$. The hybridization of light and plasma waves leads to the formation of a new collective excitation in 2DES, a plasmon–polariton. Electrodynamic effects become substantial at small wave vectors of plasmons, when their phase velocity approaches the velocity of light. For typical parameters of a semiconductor heterostructure, this happens at $q = 10\ \text{cm}^{-1}$ and a frequency of 10–30 GHz. The observation of two-dimensional plasmons at such frequencies became possible due to significant progress in molecular beam epitaxy technology. As a result, two-dimensional plasmon-polariton excitations were discovered [13–16].

A dielectric environment can strongly modify dispersion law (3). In the absence of screening by a gate, $\varepsilon(q)$ most often is a half-sum of permittivities of the vacuum and the GaAs substrate ($\varepsilon_{\text{GaAs}} = 12.8$): $\varepsilon(q) = \bar{\varepsilon} = (\varepsilon_{\text{GaAs}} + 1)/2$. In the case of practical importance, when an ideally conducting gate is located below 2DES at distance h, the effective permittivity is expressed as $\varepsilon(q) = [1 + \varepsilon_{\text{GaAs}} \coth(qh)]/2$. For a majority of semiconductor heterostructures used in experiments, condition $qh \ll 1$ is valid. With such strong screening, the spectrum of two-dimensional plasmons acquires a linear behavior [17]:

$$\omega_g = \sqrt{\frac{4\pi n_s e^2 h}{m^*\varepsilon_{\text{GaAs}}}\,q}\,. \tag{4}$$

In a magnetic field, free electrons periodically move along the cyclotron orbit with frequency $\omega_c = eB/(m^* c)$, where B is the magnetic field magnitude. The phenomenon of cyclotron diamagnetic resonance was first observed in bulk low-doped germanium and silicon semiconductors [18, 19]. This technique allowed the first reliable establishment of band structures of most semiconductors. The application of an external magnetic field perpendicular to the 2DES plane gives rise to a hybridization of the plasma and cyclotron oscillations. As a result, a cyclotron magnetoplasma mode arises with the frequency [20, 21]

$$\omega_{\text{mp}} = \sqrt{\omega_p^2 + \omega_c^2}\,. \tag{5}$$

Two-dimensional cyclotron magnetoplasma excitations have a gap in the spectrum: their frequency ω_{mp} exceeds the cyclotron frequency ω_c.

In a laterally restricted two-dimensional electron system, e.g., a disc-shaped one, subjected to a perpendicular magnetic field, alongside the cyclotron magnetoplasmon, one more plasma mode is observed, referred to as an edge magnetoplasmon [22–26]. Edge magnetoplasmons (EMPs) are collective excitations of electron density propagating along a 2DES in only one direction specified by the magnetic field and the external normal to the 2DES edge. The gapless dispersion law and the possibility of making observations at relatively low frequencies in the $\omega\tau \ll 1$ regime are characteristic features of EMPs. The latter feature allows observing EMPs at frequencies as low as 1 kHz [27]. In the semi-infinite plane model with a sharp edge, the EMP dispersion is expressed as [28]

$$\omega_{\text{EMP}} = \frac{2\pi\sigma_{xy} q}{\varepsilon}\left(\ln\frac{2}{ql} + 1\right), \qquad \omega_c\tau > 1\,, \tag{6}$$

where $\sigma_{xy} \propto n_s/B$ is a nondiagonal component of the 2DES conductivity tensor, and $l = \mathrm{i}\sigma_{xx}/2\varepsilon\varepsilon_0\omega$ is a characteristic dimension of the charge variation domain in the magnetoplasma wave. In the limit of high magnetic fields, when l becomes smaller than the depletion domain size w, it is w that should be substituted in Eqn (6) rather than l. It is worth particular attention that the charge of an edge magnetoplasmon is strongly localized near the 2DES edge. That is why in strong magnetic fields the EMP spectroscopy proved an efficient tool for studying edge current states in the modes of integer and fractional quantum Hall effects [29–34].

The aim of the present review is to present new experimental results and fields of research of collective plasma excitations in high-quality two-dimensional electron systems. The paper is organized as follows. In Section 2, we describe the original optical technique used to measure the resonant heating of 2D electrons under the excitation of a plasma wave. Section 3 discusses the behavior of 2D plasma oscillations in samples of different shapes (discs, rings, and strips) and dielectric environments. In Section 4, the spectrum and damping of plasma oscillations are studied in the long-wave limit, when a new plasmon–polariton excitation arises due to the hybridization. Section 5 describes experiments that led to the discovery of a new family of 2D plasma oscillations, metal-induced plasmons. In Section 6, plasma and magnetoplasma excitations in novel 2D materials (graphene, MgZnO/ZnO and AlGaAs/AlAs heterostructures) are studied. In the Conclusion, we discuss possible avenues of further development of experiment and theory in the field of two-dimensional plasmonics.

2. Experimental technique

To investigate the absorption of microwave and terahertz radiation, an optical technique was developed based on the high sensitivity of the luminescence spectrum of two-dimen-

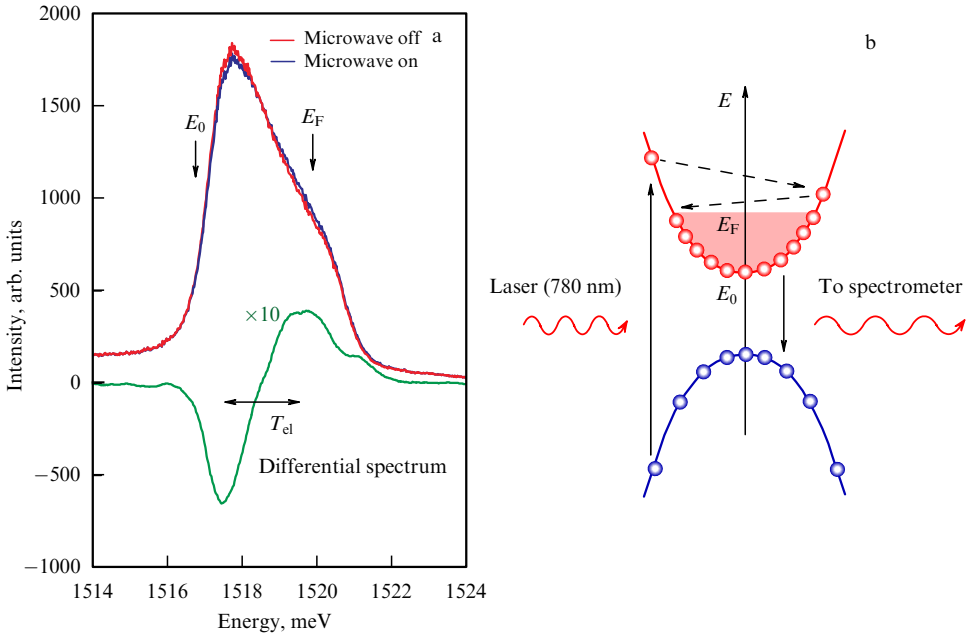

Figure 1. (Color online.) (a) Characteristic luminescence spectrum excited by microwave radiation with a power of 50 μW and a frequency of 22.5 GHz (blue curve) and without radiation (red curve). The response of a disc-shaped 2DES 1 mm in diameter with a 2D density of electrons of 0.9×10^{11} cm^{-2} in a magnetic field of 60 mT was studied. Near the Fermi energy E_F, the spectrum substantially changes under microwave excitation because of heating. The lower (green) curve plots the differential luminescence spectrum. The integral of the absolute value of the differential spectrum is a measure of microwave radiation absorption. (b) Schematic energy diagram illustrating optical transitions in the 2DES under laser irradiation.

sional electrons to resonant heating [35, 36]. This technique allows detection of 2DES heating that occurs due to the relaxation of resonantly excited plasma oscillations in the system. An important feature of this technique is the absence of any metallic electrodes (gates, contacts) near the studied structure that would inevitably affect the spectrum and damping of plasma oscillations. This property makes optical detection one of the most delicate methods of studying collective and single-particle excitations in semiconductors.

The essence of the technique is the following. The sample to be studied is irradiated by a stabilized semiconductor laser with the wavelength $\lambda = 780$ nm via a silica optical fiber 0.4 mm in diameter. The photoluminescence signal from the 2DES is collected by the same optical fiber and analyzed using a monochromator with a charge-coupled device (CCD) camera. Figure 1 illustrates the technique. As mentioned above, under heating, the luminescence spectrum of the 2DES drastically changes. An integral of the absolute value of the luminescence difference spectrum can serve as a 2DES heating measure (Fig. 1a). Figure 1b shows a schematic diagram of transitions between the energy levels that occur in the 2DES under laser exposure.

3. Plasma excitations with various dimensionalities

The physical properties of plasma oscillations can be varied within wide limits by changing the 2DES sample shape and its dielectric environment. In contrast to three-dimensional (3D) plasmons, two-dimensional plasmons are low-frequency oscillations of electron density with a gapless dispersion law. The same relates to one-dimensional (1D) plasmons implemented in 2DES strips — collective low-frequency excitations whose dispersion dependence is linear rather than quadratic root (as for 2D plasmons). Note that for plasma waves the condition of dimensionality reduction is very soft. A characteristic dimension, a comparison with which determines the dimensionality of a given sample, is the plasmon wavelength λ_p. For example, a strip of two-dimensional electrons with the width $W \ll \lambda_p$ from a point of view of collective plasma motion is an object of reduced dimension 1D, although the motion of each individual electron remains two-dimensional.

3.1 Two-dimensional plasmons in discs

Disc-shaped 2DES samples have the simplest topology and are most convenient for studying plasma excitations. The classification of plasma modes for disc geometry was first presented in the theoretical paper [37]. The modes are described by the radial l and azimuthal m numbers ($l = 1, 2, \ldots$; $m = 0, \pm 1, \pm 2, \ldots$) that characterize the number of nodes in the oscillating potential of a standing plasma wave along the radius and perimeter, respectively. Oscillations with $l = 1$ and $m = 1$ are considered the fundamental plasma mode. In most experiments on studying the properties of plasma excitations in 2DES, only the modes with $m \neq 0$ are observed, since their dipole moment is nonzero, thus making possible their efficient excitation by a plane electromagnetic wave incident on the sample.

Figure 2b shows the experimentally obtained magnetodispersion for several modes with $l = 1$ and different azimuthal numbers m [38]. The sample was a disc with diameter $d = 0.5$ mm with electron concentration $n_s = 2.6 \times 10^{11}$ cm^{-2}. In a perpendicular magnetic field, the fundamental magnetoplasma resonance (blue dots in Fig. 2b) splits into two branches. The upper one ($m = +1$) has positive magnetodispersion, and, with the increase in the magnetic field magnitude, its frequency asymptotically tends to that of the cyclotron resonance $\omega_c = eB/(m^* c)$ (m^* is the electron effective mass). This branch corresponds to the excitation of the

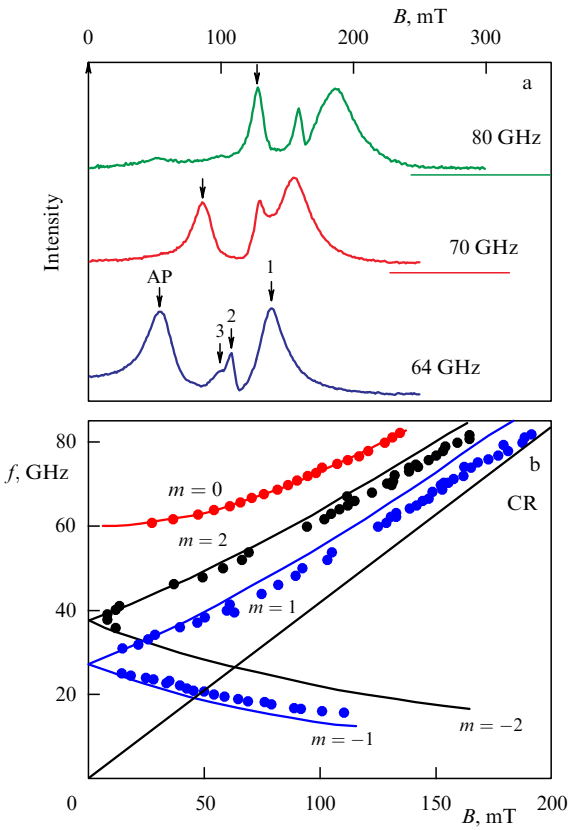

Figure 2. (Color online.) (a) Dependence of microwave absorption intensity on the magnetic field for three frequencies of microwave irradiation, 64, 70, and 80 GHz, in a 2DES disc with diameter $d = 0.5$ mm and electron concentration $n_s = 2.6\times10^{11}$ cm^{-2}. (b) Magnetodispersion of plasma modes with $m = \pm1, \pm2$ (blue and black dots) and the 'dark' mode with $m = 0$ (red dots). Blue and black curves correspond to theoretical magnetodispersion dependences according to (7); the black straight line corresponds to cyclotron resonance (CR) in GaAs.

cyclotron magnetoplasma mode. The lower branch demonstrates negative magnetodispersion and corresponds to the edge magnetoplasmon, an analog of surface plasma waves in three-dimensional electron systems. The EMPs propagate along the 2DES boundary and localize near this boundary in strong magnetic fields [22–25].

The experimental results for magnetoplasmons ($m \neq 0$) are well described by theoretical magnetodispersion dependence (blue curves in Fig. 2) [22, 39]

$$\omega = \pm\frac{\omega_c}{2} + \sqrt{\omega_p^2 + \left(\frac{\omega_c}{2}\right)^2}\,, \tag{7}$$

where ω_p is the plasma frequency in a zero magnetic field. The behavior of the multiple harmonic with $m = \pm2$ (black dots) is described by a similar dependence. Indeed, Fig. 2a shows three typical absorption curves obtained for microwave radiation frequencies 64, 70, and 80 GHz. The absorption curve measured at $f = 64$ GHz exhibits a series of already identified resonances with $m = 1$, 2, and 3. A separate resonance of an axisymmetric plasmon (AP) is also seen, whose amplitude is comparable to that of the fundamental magnetoplasma resonance. This means that the AP resonance corresponds to a special type of plasma excitation in a 2DES. Below, we will show that the AP resonance corresponds to the excitation of a plasma mode with $m = 0$, which has a zero dipole moment. For this reason, such modes are called 'dark' or axisymmetric plasmons [37]. Figure 2b shows the magnetodispersion of the mode with $m = 0$ (red dots). The magnetodispersion (red curve) is described well by the standard expression

$$\omega^2 = \omega_p^2 + \omega_c^2\,. \tag{8}$$

A characteristic feature of an axisymmetric plasma mode is that it has no edge branch in magnetodispersion. This is explained by the lack of electron density nodes along the sample perimeter ($m = 0$). Because of the zero dipole moment, such plasma oscillations cannot be excited using a uniform electromagnetic field. Therefore, the axisymmetric plasma modes are observed using near-field techniques [23, 38, 40]. The 'dark' modes are excited by metallic electrodes or optical fibers, near which an electromagnetic field with strong local nonuniformity is formed. The AP frequency in a zero magnetic field is determined by Eqn (3), where the wave vector is $q = 7.9/d$ [37].

Axisymmetric plasma excitations have a number of unique physical properties that determine their special position in the family of plasma oscillations. First, 'dark' plasma excitations have a specific magnetodispersion law without an edge branch in a perpendicular magnetic field. Second, due to the zero dipole moment, the hybridization with light and the radiative damping of axisymmetric plasmons are substantially smaller than in dipole-active 2D plasmons [40, 41]. Therefore, the 'dark' plasma modes possess a much greater Q-factor than that in ordinary plasma excitations with $m \neq 0$, which makes them an attractive subject for systems of classical and quantum plasmon electronics.

3.2 One-dimensional plasmons in strips

If a 2DES has the shape of a narrow strip with $L \gg W$, where L is the strip length and W is its width, then the dispersion of plasmons experiences a considerable modification due to the changed configuration of Coulomb interaction in the system. Indeed, the force of Coulomb attraction between opposite charges in a 2D plasma wave is $F \sim 1/\lambda_p$, whereas in a strip it is $F \sim 1/\lambda_p^2$. Thus, it becomes possible to observe one-dimensional plasma oscillations. The main difference between 1D plasmons and 2D plasmons is their linear dispersion law (with a logarithmic correction in the region of small wave vectors). The behavior of 1D plasmons is considered in theoretical papers [42–45]. The dispersion law for 1D plasmons in the model of the semi-elliptic profile of electron density distribution across the strip with width W at $qW \ll 1$ has the following form:

$$\omega^2 = \frac{2n_s e^2 W}{m^*\varepsilon}\, q^2 \left[\ln\left(\frac{8}{qW}\right) - 0.577\right], \tag{9}$$

where n_s is the concentration of electrons, ε is the effective permittivity of the medium, and m^* is the electron effective mass. The deviation from a linear dispersion law manifests itself at small wave vectors and is described by a logarithmic correction, which becomes significant in 2DES strips with a very large aspect ratio L/W of about 1000/1 [46].

The first experimental work on the detection and investigation of one-dimensional plasmons was carried out using the methods of inelastic light scattering [48] and infrared spectroscopy [47]. A drawback of these experiments was that, in order to enhance the plasma response, the

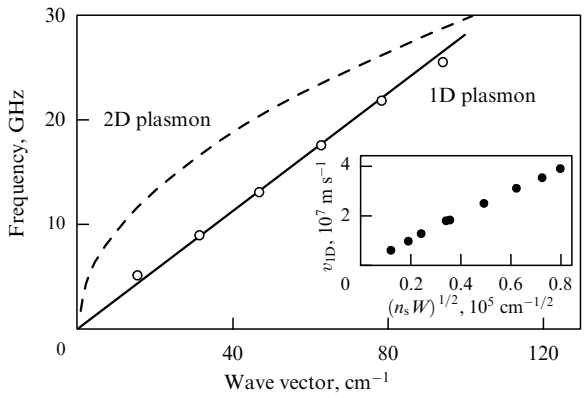

Figure 3. 1D plasmon dispersion measured in a single strip with length $L = 2$ mm and width $W = 0.1$ mm at the concentration of 2D electrons $n_s = 1.2 \times 10^{11}$ cm^{-2}. Dispersions of 2D and 3D plasmons theoretically predicted by Eqns (3) and (9) are also shown. The experimentally observed linear dispersion $\omega_p = v_{1D} q$ is a characteristic property of one-dimensional plasma excitations ($v_{1D} = 1.82 \times 10^7$ m s^{-1}). In the inset, the dependence of v_{1D} on the parameter $\sqrt{n_s W}$ is shown.

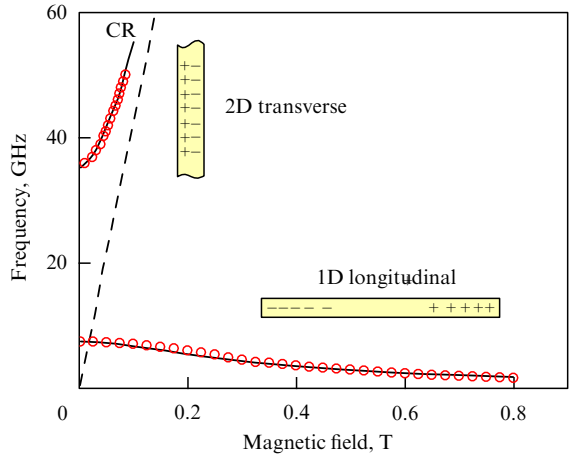

Figure 4. Magnetodispersion of the longitudinal one-dimensional and transverse two-dimensional modes measured in a 2DES strip with the dimensions 2×0.2 mm and electron density $n_s = 1.2 \times 10^{11}$ cm^{-2}. The dashed line corresponds to the cyclotron resonance.

measurements were taken in periodic arrays of nanowires rather than in individual strips. As a result, many effects characteristic of 1D plasmons were suppressed in such systems because of the interaction between the strips. Moreover, the experiments were complicated by the quantization of electron motion in the 2DES plane. Relatively recently, the optical detection method allowed observing plasma oscillations in single macroscopic electron strips [46, 49]. Figure 3 shows the spectrum of 1D plasma excitations measured in a single strip with length $L = 2$ mm, width $W = 0.1$ mm, and concentration of two-dimensional electrons $n_s = 1.2 \times 10^{11}$ cm^{-2} [49]. The spectrum was found to have a linear form $\omega_p = v_{1D} q$, which is a characteristic property of one-dimensional plasma oscillations. The circles on the dispersion plot correspond to the excitation of standing 1D plasma waves along the long side of the strip with the wave vector $q = N\pi/L$ $(N = 1, 2, \ldots)$. The inset in Fig. 3 presents the measured dependence of velocity v_{1D} on parameter $\sqrt{n_s W}$. Thus, the velocity of 1D plasmons can be tuned by varying the strip width W and electron concentration n_s.

In a magnetic field, the longitudinal 1D plasma mode demonstrates negative magnetodispersion, and in the limit of strong magnetic fields, it becomes an edge magnetoplasmon (Fig. 4). In addition to the 1D plasmon, in a 2DES strip one can observe standing plasma 2D waves corresponding to an oscillation of electron density across the strip. Such longitudinal-transverse splitting is characteristic of plasma oscillations in strip geometry. The transverse plasma 2D mode is much higher in frequency and possesses a positive magnetodispersion (see Fig. 4). Its frequency asymptotically tends to the cyclotron resonance (CR) frequency in the strong magnetic field limit. Such a behavior is characteristic of a cyclotron magnetoplasmon.

3.3 Two-dimensional plasmons with screening

In recent times, the attention of researchers has been attracted to the properties of 2D plasma waves in semiconductor structures with a gate. Such an architecture is present, e.g., in high-electron-mobility transistors (HEMTs), widely used in modern electronics. The presence of a gate near the two-dimensional channel leads to the screening of Coulomb interaction between charge carriers. This circumstance can be taken into account through the effective permittivity of the medium $\varepsilon(q)$ — the function that enters expression (3) for the dispersion of two-dimensional plasma excitations. In the presence of a metallic gate placed at distance h below a 2DES, the effective permittivity is expressed as $\varepsilon(q) = [1 + \varepsilon_{GaAs} \coth(qh)]/2$. In most experiments with modern semiconductor microstructures, the condition $qh \ll 1$ is satisfied. Under such strong screening, the velocity of 2D plasmons significantly decreases and the spectrum acquires a linear character [20]:

$$\omega_g = \sqrt{\frac{4\pi n_s e^2 h}{m^* \varepsilon_{GaAs}}}\, q\,. \tag{10}$$

This dispersion law is confirmed in many experiments [50–56]. For example, Fig. 5a illustrates the dependence of the resonance frequency on the external magnetic field magnitude [55]. The measurements were carried out in 2DES samples, where, under a quantum well at distance $h = 840$ nm, there was a back gate formed by a strongly doped (2×10^{18} cm^{-3}) n$^+$-GaAs layer 600 nm wide. The mobility of two-dimensional electrons in the quantum well was $\mu = 10 \times 10^6$ cm^2 (V s)$^{-1}$ for the concentration $n_s = 10^{11}$ cm^{-2} ($T = 4.2$ K). Two samples in the form of disk arrays with the disc diameters $d = 30$ μm and 100 μm were studied. It was found that the magnetodispersion of upper and lower screened magnetoplasma modes is best described by Eqn (7) (solid lines in Fig. 5a). In the field $B = 0$, the plasma frequency is described by Eqn (10) with the effective wave vector $q = 3.7/d$ [37], which substantially differs from the wave vector of a plasmon in the unscreened case $q = 2.4/d$ [13, 37].

Figure 5b shows the measured dependence of plasma frequency on the wave vector $q = 3.7/d$ in a zero magnetic field. The dependence is linear, which is typical exactly for plasma excitations in strongly screened 2DESs. The solid line shows the theoretical prediction for the dispersion of a screened plasmon according to Eqn (10). In relation to the experimental data presented in Fig. 5, we would like to direct the reader's attention to a peculiar feature of 2D plasma excitations in systems with strong screening. According to

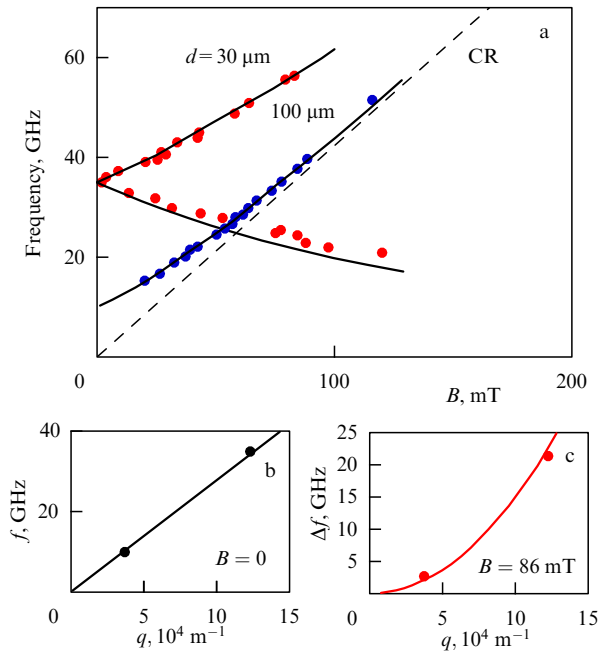

Figure 5. (Color online.) (a) Magnetodispersion of cyclotron and edge magnetoplasma modes in 2DES discs of different diameters ($d = 30$ μm and 100 μm) with strong screening. Solid lines show the theoretical curves obtained according to Eqn (7). (b) The dependence of plasma frequency on the wave vector $q = 3.7/d$ in a zero magnetic field. (c) The difference Δf between the plasma and cyclotron frequencies versus the wave vector in magnetic field $B = 86$ mT. The distance from the 2DES to a gate placed below the quantum well is $h = 840$ nm. The concentration of two-dimensional electrons in the 2DES is $n_s = 10^{11}$ cm^{-2}.

Eqn (7), which perfectly describes experimental data, the cyclotron magnetoplasma mode frequency in the limit $\omega_c \gg \omega_p$ is determined by the expression $\omega = \omega_c + \omega_p^2/\omega_c$. Substituting the screened plasmon frequency ω_p from Eqn (10) into this expression, we find

$$\hbar\omega = \hbar\omega_c + \frac{\hbar^2 q^2}{2m_p}\,, \qquad m_p = \frac{\hbar\varepsilon_0\varepsilon}{2n_s e a}\,B\,. \tag{11}$$

From (11), it follows that the dependence of energy on the wave vector for a cyclotron screened plasmon is quadratic and has a gap ω_c. Therefore, a screened magnetoplasmon can be associated with a quasiparticle having the mass m_p. The mass of such a quasiparticle can easily vary within a wide range by changing the external magnetic field. As an example, Fig. 5c presents the experimental dependence of the frequency difference $\Delta f = f - f_c$ on the plasmon wave vector q in the magnetic field $B = 86$ mT. In the same figure, the solid line shows an approximation of the experimental data by a quadratic function. The plasmon quasiparticle mass value extracted from this approximation amounts to $m_p = 1.2 \times 10^{-5} m_0$. Since plasma excitations obey the Bose–Einstein statistics, such a small mass makes the new quasiparticle a promising candidate for studying various effects, e.g., Bose–Einstein condensation.

One more frequently used method of changing the velocity of 2D plasma excitations is 2DES lateral (side) screening, implemented, for example, in a gap diode, where a two-dimensional channel is gripped in a plane between two well-conducting contacts. Theoretical consideration shows that the lateral screening considerably modifies the position, width, and amplitude of the plasma resonance [57–60]. Indeed, in experiment [61], it was demonstrated that the presence of a lateral (side) metallic gate markedly 'softens' the frequency of two-dimensional plasma excitations (up to $\omega_{exp}/\omega_p = 2$). In this case, the lateral screening effect is shown to increase with a reduction in 2DES size, which is evidence of a difference between the dispersion law of laterally screened plasmons and the square root law (3). The effect turned out to be related to the electrodynamic renormalization of the plasmon spectrum in a laterally screened 2DES [60].

4. Plasmon–polariton excitations

Electrodynamic effects in a two-dimensional plasma caused by the finiteness of the speed of light $c = 3 \times 10^8$ m s^{-1} are increasingly attracting the interest of researchers. On the one hand, the retardation effects become significant when the wavelength of the electromagnetic radiation appears comparable to the structure size. In this case, plasmon polaritons, i.e., coupled states of light with 2D plasmons, appear [13–16, 62, 63]. The influence of the electrodynamic effect can be quantitatively described by the retardation parameter A defined as the ratio of the 2D plasmon frequency ω_p in the quasistatic approximation to the light frequency $\omega_{light} = cq/\sqrt{\varepsilon}$ in the medium with the same wave vector q [7]. Therefore,

$$A = \frac{\omega_p(q)}{\omega_{light}(q)} = \sqrt{\frac{n_s e^2}{2m^*\varepsilon_0}\,q}\,\frac{1}{\omega_{light}(q)} \sim \sqrt{\frac{n_s}{q}}\,. \tag{12}$$

On the other hand, the interaction of the two-dimensional plasma with light can be essential also because of the radiative damping of the synchronous oscillation of charge carriers in the plasma wave. The radiative damping mainly affects the plasma resonance width. Theoretical calculations predict that, for an infinite-plane 2DES in a vacuum, the plasma resonance width is determined by the sum of the incoherent collision contribution $\gamma = 1/\tau$, characterized by the scattering time τ, and the radiation term $\Gamma = \gamma 2\pi\sigma_{2D}/c$ [11, 12, 64–67],

$$\Delta\omega = \gamma + \Gamma = \frac{1}{\tau}\left(1 + \frac{2\pi\sigma_{2D}}{c}\right). \tag{13}$$

As seen from Eqn (13), the effect of radiative damping on the plasmon resonance width is determined by the dimensionless relativistic parameter $2\pi\sigma_{2D}/c$. Here, $\sigma_{2D} = \mu n_s e$ is the static two-dimensional conductivity of the 2DES. When $2\pi\sigma_{2D}/c \gg 1$, the radiative effects become appreciable. Note that, for typical parameters of current heterostructures $n_s = 10^{11}$ cm^{-2} and $\mu = 10^7$ cm^2 (V s)$^{-1}$, we get $2\pi\sigma_{2D}/c = 30$. Thus, the radiative effects are virtually always to be taken into account [62].

4.1 Retardation effects

Retardation effects become substantial at $q \approx 2\pi n_s e^2/m^* c^2$ and $\omega \approx 2\pi n_s e^2/m^* c\sqrt{\varepsilon}$, when the phase velocity of plasmons from Eqn (3) becomes comparable to the velocity of light. For typical parameters of semiconductor AlGaAs/GaAs heterostructures ($n_s = 3 \times 10^{11}$ cm^{-2}, $m^* = 0.067 m_0$, $\varepsilon = 12.8$), such a situation takes place at $q \approx 10$ cm^{-1} and the frequency $\omega/(2\pi) \approx 30$ GHz. The observation of 2D plasmons at such low frequencies was impossible in the early years of two-

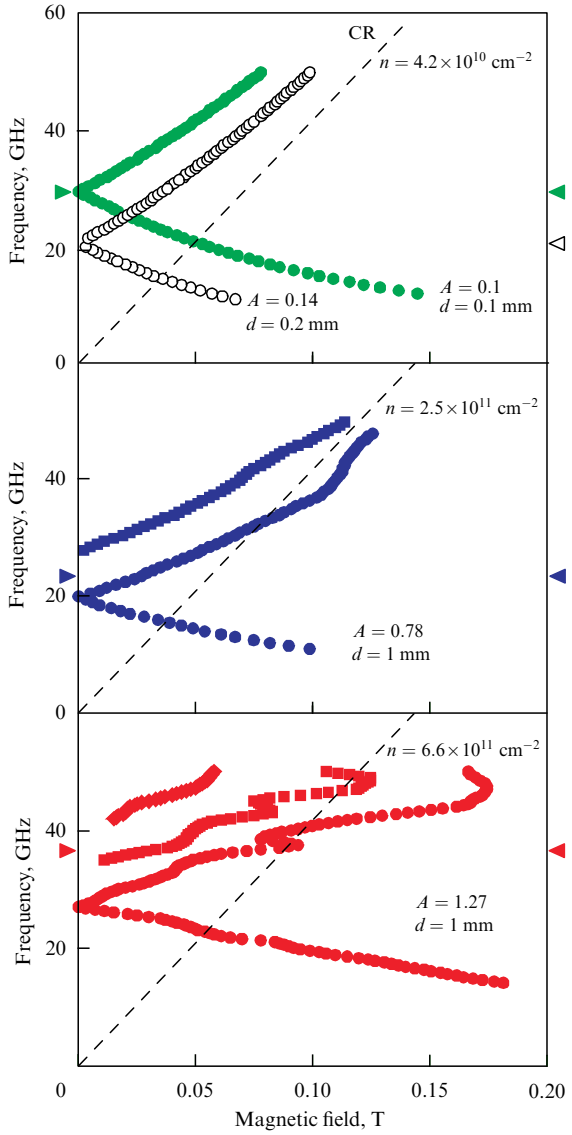

Figure 6. Spectra of two-dimensional magnetoplasmons at a temperature of 1.5 K for several single-disc samples with different electron densities and mesa diameters. For each of the samples, the value of retardation parameter A is presented. Arrows point to the values of plasma frequency obtained in the electrostatic approximation according to Eqn (3).

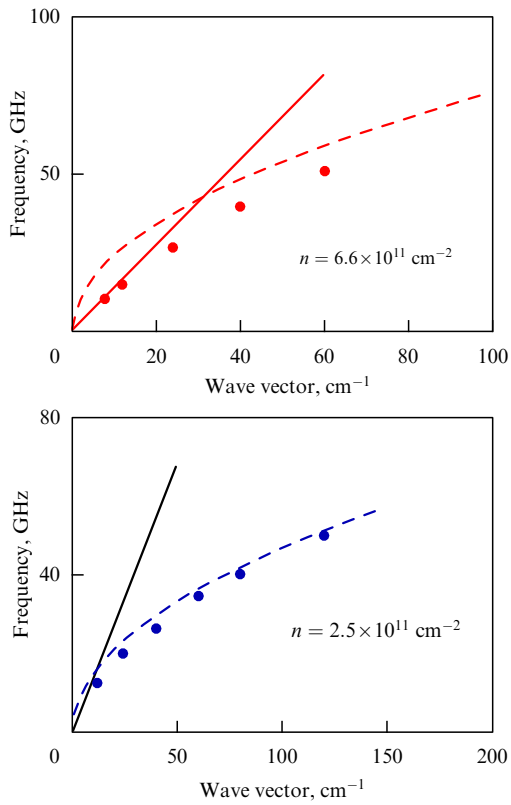

Figure 7. Dispersion of plasmon–polariton 2D excitations measured in disc-shaped samples with electron density $n_s = 6.6 \times 10^{11}$ cm^{-2} and $n_s = 2.5 \times 10^{11}$ cm^{-2}.

dimensional plasmonics (1970s–1980s), because — in the structures used at that time — the relaxation time determined the lower boundary of the plasma excitation frequency at the level of 100 GHz. In the few last decades, the quality of samples has radically improved, making possible the observation of hybrid plasmon–polariton modes [13–16]. These experiments revealed interesting and unexpected properties of plasmon–polariton 2D excitations. In the regime of strong influence of retardation effects, a considerable decrease in the resonance plasma frequency was demonstrated, alongside the extremely unusual zigzag magnetic-field behavior of the dispersion.

Figure 6 presents the magnetic field dependences of the absorption resonance frequency of 2DES discs with diameter $d = 0.1$ and 1 mm and with an electron concentration of $(0.42-6.6) \times 10^{11}$ cm^{-2} [13]. Arrows indicate the frequency values calculated using the quasistatic approximation (3). With the increasing retardation parameter A, several features are observed: (1) the plasmon frequency in a zero magnetic field considerably decreases compared to ω_p calculated in the quasistatic approximation; (2) the slope $|d\omega_\pm/d\omega_c|$ at $B \to 0$ becomes significantly smaller than the standard value of $1/2$; (3) the upper magnetoplasma mode crosses the cyclotron resonance line and demonstrates unusual zigzag behavior. Let us consider these features one by one.

Figure 7 shows the frequency of a plasmon–polariton 2D excitation in a zero magnetic field measured as a function of the wave vector $q = 2.4/d$. The dependences are obtained for two discs with electron concentrations $n_s = 2.5 \times 10^{11}$ cm^{-2} and $n_s = 6.6 \times 10^{11}$ cm^{-2}. The same figure shows the dispersion of light $\omega = 2\pi f = cq/\sqrt{\varepsilon}$ (solid curve) and 2D plasmon $\omega = 2\pi f = (2\pi n_s e^2 q/m^* \bar{\varepsilon})^{1/2}$ (dashed curve). In the limit of small wave vectors (large wavelengths), the spectrum of plasmon–polariton excitations is seen to tend to the dispersion of light, whereas in the short-wave limit the plasmon–polariton spectrum is well described by the electrostatic approximation (3). It is because of the hybridization with the light wave in the limit of small wave vectors that the considerable decrease in the plasmon frequency in a zero magnetic field occurs. The hybridization with light also explains the decrease in the slope $|d\omega_\pm/d\omega_c|$ of magnetodispersion curves at $B \to 0$. Indeed, the light wave magnetodispersion plotted as $f(B)$ is a horizontal straight line.

The physical reason for the unusual zigzag behavior of the cyclotron magnetoplasma mode is the interaction between the fundamental mode and the multiple magnetoplasma harmonics [63]. Indeed, it is experimentally shown that with the increase in the magnetic field when approaching the cyclotron resonance the amplitude of the fundamental mode decreases, whereas the second harmonic amplitude, on the contrary, increases [13, 14]. This is due to the competition

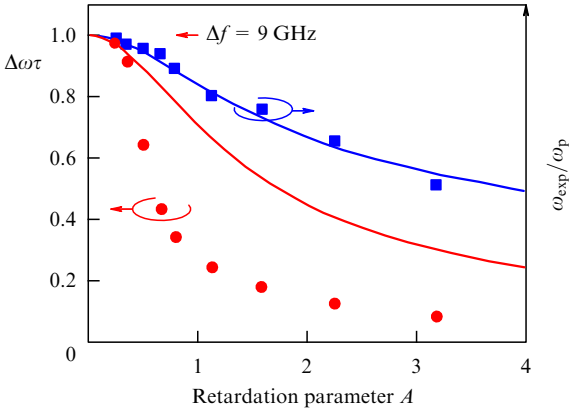

Figure 8. (Color online.) The normalized plasmon damping $\Delta\omega\tau$ (red dots) and frequency $\omega_{\rm exp}/\omega_{\rm p}$ as functions of the retardation parameter A. The solid curves show the theoretical prediction for a 2DES with infinite size in the plane.

between the collisional γ and radiation Γ contributions to the plasma resonance width. Since in the experiments the magnetic field is swept while the frequency of microwave radiation is fixed, the predominance ('winning') of amplitudes of different magnetoplasma modes manifests itself as a zigzag in the magnetodispersion dependence. Note that the discovered zigzag behavior is a delicate effect and can be observed only in top-quality samples, when $\gamma \ll \omega_{\rm p} < \Gamma$ [63].

A characteristic of plasma oscillations of primary importance is their damping, which manifests itself through the plasma resonance linewidth. This issue is closely related to the problem of practical application of 2D plasmonics in detecting and generating terahertz radiation. Two-dimensional plasma modes are resonantly excited only when $\omega_{\rm p}\tau \gg 1$. This circumstance allows resonant excitation of plasma waves in modern semiconductor heterostructures only at cryogenic temperatures. One of the ways to avoid this limitation is to increase the effective scattering time τ by coupling the plasma wave with light.

In Fig. 8, the red dots show the dependence of the plasma resonance half-width normalized to $1/\tau$ on the retardation parameter A obtained in [16]. Blue squares demonstrate the normalized plasmon frequency $\omega_{\rm exp}/\omega_{\rm p}$ versus the retardation parameter. Here, $\omega_{\rm exp}$ is the experimental value of the plasma frequency in a zero magnetic field, and $\omega_{\rm p} = [2\pi n_{\rm s} e^2 q/(m^* \overline{\varepsilon})]^{1/2}$ is the plasma frequency calculated in the electrostatic approximation. The measurements were performed with a sample of a 2DES with the electron concentration $n_{\rm s} = 6 \times 10^{11}$ cm^{-2} and relaxation rate $1/\tau = 5.6 \times 10^{10}$ s^{-1}. According to the data presented in Fig. 8, the plasmon resonance experiences significant narrowing even at minor hybridization with light. Solid curves in the figure show the theoretical dependences, obtained under the assumption that the 2DES dimensions in the plane are infinite [68]. In the limit $A \ll 1$, these dependences are described by the expressions

$$\omega^2 = \frac{\omega_{\rm p}^2}{1 + 0.5\,A^2}\,, \qquad \Delta\omega = \frac{1}{\tau}\,\frac{1}{1 + 0.5\,A^2}\,. \tag{14}$$

The experimental points for $\omega_{\rm exp}/\omega_{\rm p}$ are perfectly described by the theory, whereas the half-width of the plasmon–polariton resonance $\Delta\omega\tau$ experiences a much greater decrease than predicted by theory. Such anomalous behavior is probably because the studied 2DES disc-shaped sample has a finite size, which is not taken into account in the theoretical model.

It is interesting to construct a qualitative theory of the observed plasma resonance narrowing. In the direction perpendicular to the 2DES plane, the plasma wave field is concentrated in the region λ_z. If the retardation can be disregarded, then $\lambda_z = \lambda_{\rm p} = 2\pi/q$ and the plasma resonance half-width is $\Delta\omega = 1/\tau$. When the retardation is great, the plasma wave delocalization λ_z greatly exceeds the region $\lambda_{\rm p} = 2\pi/q$ where the dissipation occurs [68]. Hence, the damping of a 2D plasmon–polariton excitation can be estimated using the expression

$$\Delta\omega = \frac{1}{\tau}\,\frac{\lambda_{\rm p}}{\lambda_z}\,. \tag{15}$$

The delocalization of a plasmon mode in the direction perpendicular to the 2DES plane is defined as $q_z = \sqrt{q^2 - \omega^2/c^2}$. This expression is a direct consequence of the Maxwell equations for a bounded electromagnetic wave propagating along a two-dimensional electron system, $\Delta\mathbf{E} = (\omega^2/c^2)\,\mathbf{E}$. Combining equations (2) and (15), it is possible to reproduce exactly Eqn (14) for the half-width $\Delta\omega\tau$ and frequency $\omega/\omega_{\rm p}$ of the plasma resonance. It is worth noting that Eqn (15) resembles the famous law of suppressing the spontaneous radiation of atoms placed in a resonator. This effect was first predicted by Purcell [69]. Such a coincidence is not accidental; it follows from the universal nature of all electrodynamic phenomena.

To conclude, note that a distinctive feature of plasmon polaritons is the very strong coupling between the electromagnetic field of light and the plasma (see Fig. 7). If a 2DES is placed in a resonator, it is possible to observe the ultra-strong coupling regime, when the energy of light-plasma coupling (the Rabi frequency) becomes comparable to the frequencies of noninteracting waves [70–72]. Currently, the physics of the ultra-strong coupling regime is a subject of intense studies. Particular interest in this issue is related to numerous applications in quantum optics and quantum computing [72].

4.2 Radiative damping

The second manifestation of electrodynamic effects in a 2DES is the radiative damping of plasma excitations. As shown in Section 4.1, the plasma resonance width is determined by the sum of the incoherent collisional contribution $\gamma = 1/\tau$ and the radiation part $\Gamma = \gamma 2\pi\sigma_{\rm 2D}/c$: $\Delta\omega = \gamma + \Gamma$. Here, the electrodynamic term describes the coherent dipole radiation of electromagnetic waves by oscillating two-dimensional electrons. The quantity Γ determines the probability of electron–photon scattering and plays a fundamental role in the light–matter interaction. Since radiative damping is due to a coherent collective radiative process, it is in full analogy with the Dicke 'superradiance' decay [73].

An expression for the radiative damping Γ can be qualitatively derived from the following considerations [65]. Let the studied sample have the shape of a disc with diameter d. The incident electromagnetic wave forces the 2DES electrons to oscillate coherently with the frequency ω. Each oscillating electron is a dipole that radiates with the intensity $I \sim \ddot{p}^2/c^3 \sim \omega^4 e^2 a^2/c^3$, where a is the oscillation amplitude, and $p \sim ea$ is the corresponding dipole moment. The magnitude of radiative damping Γ_0 for an individual oscillating electron is determined by the ratio of dipole

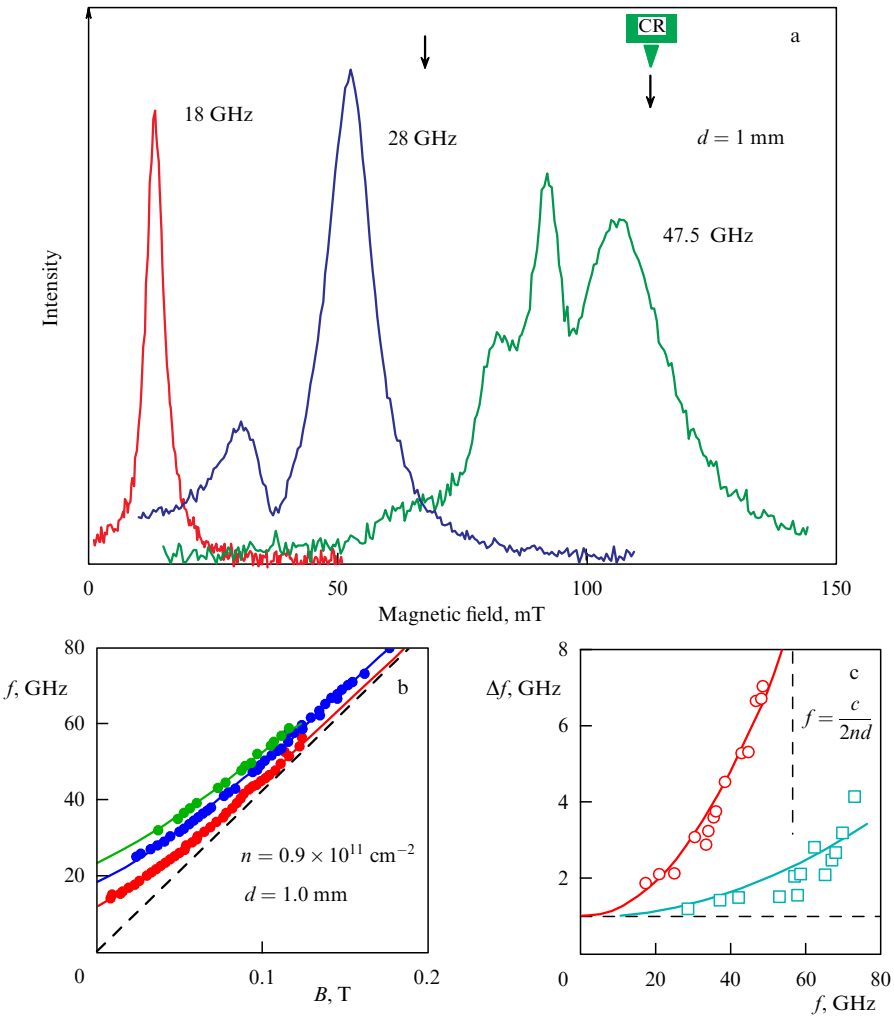

Figure 9. (Color online.) (a) Dependence of the microwave absorption intensity on the magnetic field for microwave irradiation frequencies of 18, 28, and 47.5 GHz for a sample with electron density $n_s = 0.9 \times 10^{11}$ cm^{-2} and diameter $d = 1$ mm. The arrows point to the position of cyclotron resonance. The measurements were carried out at temperature $T = 4.2$ K. (b) Magnetodispersion of the first three harmonics of the cyclotron magnetoplasma mode. The dashed line corresponds to the cyclotron resonance in GaAs. (c) Frequency dependences of the resonance line half-width Δf for the first (circles) and second (squares) magnetoplasma modes.

radiation intensity I to the electron energy $m^*\omega^2 a^2$, which yields $\Gamma_0 \sim e^2\omega^2/(m^*c^3)$. For N coherently oscillating electrons, the radiation intensity should be multiplied by N^2, and the mean energy by N, so that $\Gamma_{\text{disk}} \sim N\Gamma_0$. The total number of coherent electrons in the 2DES is $N \sim n_s d^2$, which yields the expression

$$\Gamma_{\text{disk}} \sim \Gamma \frac{d^2}{\lambda_p^2}, \qquad d \ll \lambda, \tag{16}$$

where $\Gamma = \gamma 2\pi\sigma_{2D}/c$ is the frequency-independent radiation width. In the case of an infinite-size 2DES, for the fundamental plasmon–polariton mode $d \approx \lambda$, then $\Gamma_{\text{disk}} \approx \Gamma$.

Figure 9a presents typical dependences of microwave absorption on the magnetic field, measured in a sample with diameter $d = 1$ mm and electron density $n_s = 0.9 \times 10^{11}$ cm^{-2}. At low frequencies ($f = 18$ GHz), one peak of resonance microwave absorption is observed that shifts towards greater magnetic fields as the frequency grows. This resonance corresponds to the excitation of the cyclotron magnetoplasma mode in the disc studied. The second peak arises in the frequency region above 20 GHz and the third one in the region above 30 GHz. These peaks correspond to the excitation of higher harmonics of the cyclotron magnetoplasma resonance with $m = 2$ and $m = 3$. When proceeding to higher magnetic fields and higher frequencies, all observed modes strongly broaden due to radiative damping.

For quantitative studies of the observed broadening of magnetoplasma modes, their half-width Δf was calculated from the half-width ΔB of resonances with respect to magnetic field and the slope $\partial f/\partial B$ of the magnetodispersion curves (Fig. 9b). The Δf dependence on the plasma resonance frequency obtained in this way is presented in Fig. 9c. The circles correspond to the fundamental magnetoplasma mode, and the squares correspond to its second harmonic. It is seen that in the region of low frequencies the half-width values of both the fundamental mode and the second harmonic tend to the fixed nonzero value $\Delta f = 1$ GHz. The relaxation of magnetoplasma excitation in this limit is apparently due to incoherent collisional scattering and $\Delta\omega = \gamma = 1/\tau$. However, when moving to the frequency region $f \sim c/nd$ (n is the effective refractive index of the medium surrounding the 2DES), an unexpectedly rapid increase in the width of magnetoplasma modes is observed, in which the first mode rapidly broadens and vanishes, giving way to the second one, etc. The broadening of plasma modes with the increase in the

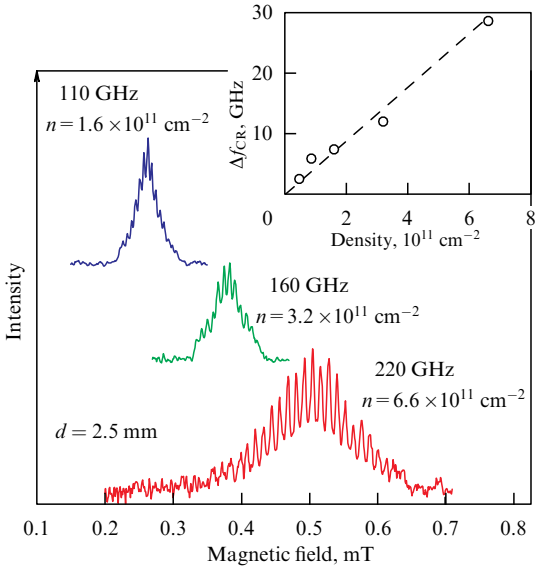

Figure 10. Microwave absorption as a function of the magnetic field, measured at high microwave frequencies for three samples with concentrations $n_s = 1.6 \times 10^{11}$ cm^{-2}, 3.2×10^{11} cm^{-2}, and 6.6×10^{11} cm^{-2}. All samples had a similar disc geometry with diameter $d = 2.5$ mm. For clarity, the curves are vertically shifted. The inset shows the dependence of the cyclotron resonance half-width Δf_{CR} on the electron concentration. The dashed line in the inset shows the theoretical dependence (17).

microwave frequency is well described by the theoretical quadratic dependence (16) depicted in Fig. 9c for each of the modes by solid curves.

At higher frequencies, when $d \geqslant \lambda$, in high-quality samples the relaxation of plasma oscillations is determined by the radiation relaxation channel. Figure 10 shows the absorption curves measured in three geometrically similar samples (discs with diameter $d = 2.5$ mm) having different electron concentrations, $n_s = 1.6 \times 10^{11}$ cm^{-2}, 3.2×10^{11} cm^{-2}, and 6.6×10^{11} cm^{-2}. The magnetoplasma cyclotron resonance undergoes significant broadening under the increase in the electron density. The inset in Fig. 10 shows the half-width extracted from these curves versus the electron density. The experimental points perfectly coincide with the theoretical dependence

$$\Delta\omega = \Gamma = \frac{2\pi\sigma_{xx}}{\bar{n}c}\,\gamma = \frac{4\pi n_s e^2}{m^*(1 + n_{\mathrm{GaAs}})c}\,. \qquad (17)$$

Here, we have taken into account the presence of a GaAs semiconductor substrate that forms the dielectric environment of the 2DES with effective refractive index $\bar{n} = (1 + n_{\mathrm{GaAs}})/2$.

5. New family of two-dimensional plasma excitations induced by metal proximity

The problem of electromagnetic wave propagation along a metallic wire was solved more than 100 years ago by Sommerfeld [42], who showed that an electromagnetic wave propagates along a wire with the speed of light. It is these plasmon polariton waves that carry alternating signals along present-day transmission lines. Recently, it was found that if a metallic wire is placed near a 2DES, then in such a hybrid system a new family of plasma excitations arises [74–80]. These so-called proximity plasmons possess a number of unique physical properties. In particular, their dispersion combines characteristic features of both screened ($\omega_{\mathrm{pr}} \propto \sqrt{h}$) and unscreened ($\omega_{\mathrm{pr}} \propto \sqrt{q}$) two-dimensional plasmons [78]:

$$\omega_{\mathrm{pr}}(q) = \sqrt{\frac{8\pi n_s e^2 h}{m^*\varepsilon}\,\frac{q}{W}}, \qquad qW \ll 1\,, \qquad (18)$$

where W is the width of the metallic gate strip placed above the 2DES at distance h, q is the wave vector of the plasma wave directed along the strip, and ε is the permittivity of the semiconductor substrate.

There are two reasons for which the observation of proximity plasma modes has been hindered over the past 50 years. First, the new plasma oscillations have no nodes in the direction perpendicular to the metallic strip, which makes it impossible to excite these modes with an electromagnetic wave whose electric field is directed across the strip. Note that this is exactly the configuration used in pioneering 2D plasmonics experiments [9, 10, 81, 82]. Second, the theoretical studies preceding the discovery of the new family of plasmon modes mainly considered the finite-size 2DES geometry with an infinite screening gate [37]. This geometry is opposite to that needed for the proximity plasmon observation. That is why there were no theoretical predictions of the existence of new waves for a long time.

5.1 Proximity plasma excitations

As mentioned above, new plasma excitations are observed in a hybrid system where a metallic gate is placed in the immediate proximity of the 2DES. In experiments on detecting new modes, a gate (70 Å Ni, 1000 Å Au) with width $W = 20-100$ μm and length $L = 0.5-1.7$ mm was used. On both sides of the strip at a distance of 0.2–0.5 mm the grounded contacts to the 2DES were made (see the inset in Fig. 11b). Figure 11a shows the curves of microwave absorption versus the magnetic field measured at frequencies of 6.7, 7.7, and 11 GHz. The curves demonstrate a pronounced resonance corresponding to the excitation of new plasma modes with the transverse wave number $N = 0$. The measurements were carried out on a structure with the gate length $L = 0.5$ mm and width $W = 0.1$ mm ($n_s = 2.7 \times 10^{11}$ cm^{-2}). Additional experiments have shown that, without a central metallic gate, this mode is not observed. This observation shows that it is the metal proximity that gives rise to the new plasma mode. The magnetodispersion of the discovered resonance is shown in Fig. 11b by red dots. In accordance with the theoretical prediction, the detected plasma mode has no edge branch, and the magnetodispersion of the cyclotron mode has a standard quadratic form (sold curve in Fig. 11b):

$$\omega = \sqrt{\omega_{\mathrm{pr}}^2 + \omega_{\mathrm{c}}^2}\,. \qquad (19)$$

Extrapolation of dispersion to the region of the zero magnetic field yields the plasma frequency $f_{\mathrm{p}}(0) = 4.8$ GHz. This value is in perfect agreement with the theoretical prediction (18), provided that the longitudinal wave vector $q = 2\pi/L$ and $\varepsilon = \varepsilon_{\mathrm{GaAs}} = 12.8$.

In addition to the fundamental longitudinal plasma mode ($N = 0$) described above, transverse plasma harmonics are also observed in experiment (circles in Fig. 11b). The transverse modes have N nodes in the variable potential of the standing plasma wave for the same longitudinal wave vector $q = 2\pi/L$. The spectrum of the transverse plasma modes in

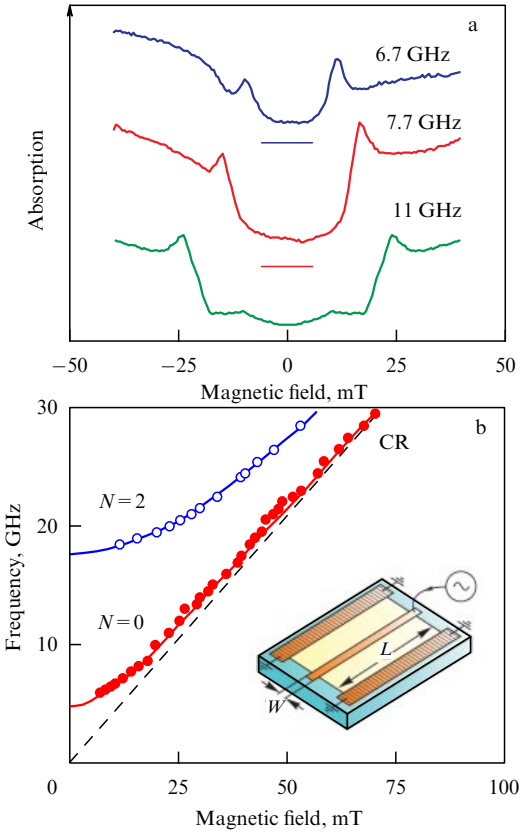

Figure 11. (Color online.) (a) Microwave absorption as a function of magnetic field measured at the three frequencies indicated in the figure. For clarity, the curves are vertically shifted. (b) The magnetodispersion of proximity plasmon modes with transverse wave number $N = 0$ (red dots) and $N = 2$ (circles). The inset shows the geometry of the structure under study.

the limit $qW \ll 1$ is described by the following expression [78]:

$$\omega^2 = \frac{4\pi n_s e^2 h}{m^* \varepsilon}\left(q_{tr}^2 + \frac{4}{W}\,q\right), \qquad (20)$$

where $q_{tr} = N\pi/W\,(N = 1, 2, \ldots)$ is the transverse component of the wave vector, and $q = 2\pi/L$ is longitudinal component of the wave vector. Note that, in the limit of large longitudinal wavelengths, Eqn (20) transforms into a standard expression (10) for a screened 2D plasmon. It is exactly this plasma mode that was observed in many experiments [50, 52–54, 56]. However, the fundamental plasma mode with $N = 0$ was missed in all these experiments.

In Fig. 11b, the transverse plasma mode corresponds to the excitation of a harmonic with the number $N = 2$. In the coplanar waveguide under study, due to the axial symmetry of the electric field, only the plasma modes with even transverse wave number $N = 2, 4, \ldots$ are excited. The experimental data for the mode $N = 2$ can be extrapolated to the region $B = 0$ using theoretical expression (19). The resulting plasma frequency of 18 GHz agrees fairly well with the theoretical prediction of 21 GHz in accordance with Eqn (20).

The most remarkable physical property of the discovered plasma excitation is its square root dispersion law [78]. At first glance, this seems unnatural, since the plasmon has a one-dimensional character of propagation along the gate, which screens the Coulomb interaction. Both of these factors should favor a linear dispersion of the plasma excitation [49, 52]. The

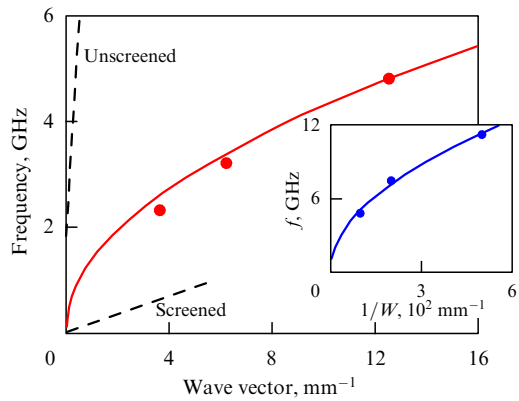

Figure 12. Dispersion of proximity plasma excitation. Each of the experimental points is measured on a separate sample with gate length $L = 0.5$, 1.0, and 1.7 mm at fixed gate width $W = 100$ μm. The electron concentration for all three samples $n_s = 2.7 \times 10^{11}$ cm^{-2}. The theoretical square root dependence (18) is shown by a solid curve. For comparison, the dispersions of usual screened and unscreened plasmons are also presented. The inset shows the dependence of the plasma frequency on the parameter $1/W$.

spectrum of the new plasmon was experimentally determined in a series of structures with different lengths of the central gate, $L = 0.5$, 1.0, and 1.7 mm, the width being fixed at $W = 100$ μm. The dispersion found in these experiments is shown in Fig. 12. For each of the experimental points, the wave vector was calculated as $q = 2\pi/L$. In the same figure, the solid line shows the theoretical dependence corresponding to Eqn (18). The experimental data are seen to completely confirm the root dispersion law predicted by theory. The inset in Fig. 12 presents the measured dependence of the new plasma mode $N = 0$ frequency on the parameter $1/W$. Each of the experimental points corresponds to a measurement on an individual structure with a definite gate width $W = 100$, 50, or 20 μm for the fixed length $L = 0.5$ mm. The experiment confirms the theory (18), according to which the plasmon frequency ω_{pr} is proportional to $1/\sqrt{W}$ (solid curve in the inset in Fig. 12).

It is remarkable that the semiconductor structure geometry studied in the present experiments closely resembles the HEMT geometry. The HEMT is shown to be applicable to the detection and generation of radiation in the terahertz frequency region (0.1–1 THz) [83–87]. The idea of the approach is that the electromagnetic wave incident on the structure transforms into a standing plasma wave localized under the gate. The alternating potential of the plasma excitation is rectified in the same structure into the measured DC photovoltage signal. However, in spite of many years of experimental efforts, terahertz plasmonic components are still far from practical implementation. Thanks to their unique physical properties, the proximity plasma excitations can play an important role in implementing systems of terahertz electronics. Indeed, their plasma frequency for typical HEMT parameters $L = 10$ μm, $W = h = 0.2$ μm, and $n_s = 10^{12}$ cm^{-2} amounts to $f_{pr} \approx 0.7$ THz.

5.2 Relativistic plasma excitations

In the structures with a closely located metallic gate described in Section 5.1, one more kind of plasma excitation, namely, a relativistic plasmon, was found [74–76]. The most important distinctive feature of the discovered mode is that its width $\Delta\omega$ is significantly smaller than the inverse relaxation time of two-

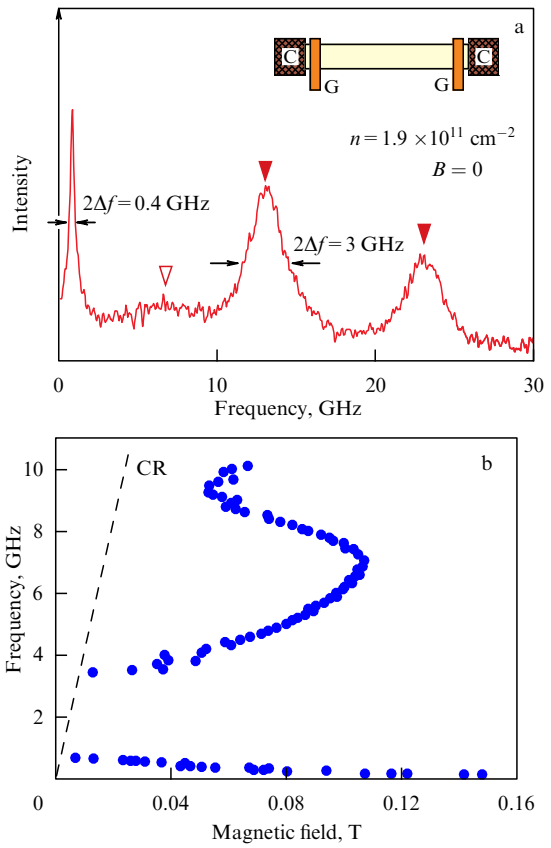

Figure 13. (a) Absorption spectrum of a 2DES strip with electron density $n_s = 1.9 \times 10^{11}$ cm^{-2} in a zero magnetic field. The inset schematically shows the sample used. (b) Magnetodispersion of a weakly-damped relativistic plasma mode measured in the same sample.

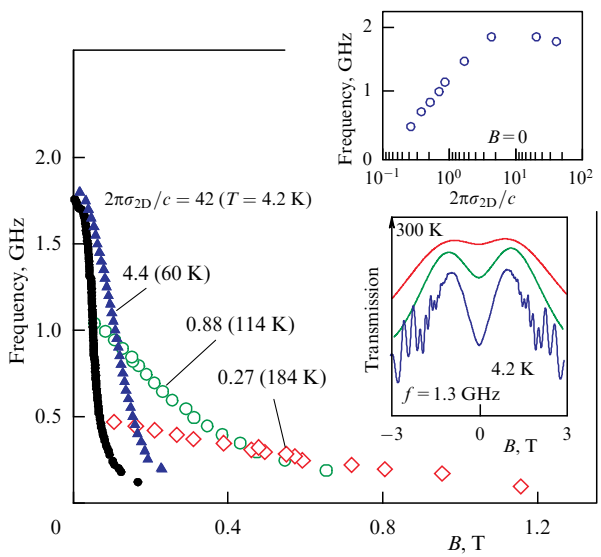

Figure 14. Magnetodispersion of an edge relativistic plasma mode at different temperatures. The upper inset shows the mode frequency in a zero magnetic field versus the relativistic parameter $2\pi\sigma_{2D}/c$. The lower inset presents the plasma relativistic resonance measured at $T = 4.2$, 160, and 300 K in a structure with an electron concentration of 4.4×10^{12} cm^{-2} at frequency $f = 1.3$ GHz

dimensional electrons, $1/\tau$. The usual plasma modes observed in the same structure possess a frequency width an order of magnitude greater. For example, Fig. 13a shows the absorption spectrum of a strip of two-dimensional electrons with a width of 100 μm and a length of 1 mm, on both sides of which ohmic contacts C are fabricated. Above the mesa at a distance of 10 μm from the contacts across the strip, metallic gates G 30 μm wide are placed to excite plasmons. The spectrum is obtained in a zero magnetic field with frequency varied in a sample with concentration $n_s = 1.9 \times 10^{11}$ cm^{-2} and distance from the crystal surface to the quantum well $h = 200$ nm.

Figure 13a demonstrates four peaks, two of them (pointed to by arrows) at frequencies $f = 13$ and 23.5 GHz correspond to the excitation of a longitudinal 1D plasma mode along the strip. Equation (9) yields values for the frequencies of the two lowest one-dimensional plasma modes that agree well with the experimental data. A small peak at the frequency of 7 GHz (pointed to by the hollow arrow) corresponds to the plasma resonance excitation considered in detail in Section 5.1. The position of this resonance perfectly agrees with Eqn (18).

The fourth peak at frequency $f = 0.8$ GHz is an unexpected observation. First, its frequency is much lower than that of any possible plasma excitations in the system being studied. Second, the revealed plasma resonance has a substantially smaller frequency width ($2\Delta f = 0.4$ GHz) than the width $2\Delta f = 3$ GHz of the resonance attributed to a one-dimensional plasmon. The unusual narrowing of the new plasma excitation becomes understandable after measuring its magnetodispersion. Figure 13b shows the dependence of the resonant plasma absorption frequency on the magnetic field magnitude. In a finite magnetic field, two modes — the edge one and the cyclotron one — are observed. The tiny slope of the cyclotron magnetoplasma branch evidences the abnormally strong influence of retardation effects on it. This is surprising, because, if we estimate the retardation parameter value for the new plasma mode from the size of its localization in the structure and the density of two-dimensional electrons, we will get $A \approx 0.1$. It is the strong hybridization with light that explains so weak a damping of the new low-frequency plasma excitations.

It is known that in the strongly retarded regime a key parameter that determines the behavior of plasma waves is the ratio of the two-dimensional conductivity $2\pi\sigma_{2D}$ and the velocity of light c [68]. Two-dimensional plasmon–polaritons in the strongly retarded regime exist when the relativistic parameter $2\pi\sigma_{2D}/c > 1$. That is why the new weakly damped plasma mode was called a 'relativistic plasmon' [75]. To investigate the influence of parameter $2\pi\sigma_{2D}/c$ on the properties of the relativistic plasma mode, measurements of edge mode magnetodispersion were carried out at various temperatures $T = 4.2-188$ K (Fig. 14). The experiments were performed in the identical geometry of the structure with $n_s = 2.4 \times 10^{11}$ cm^{-2} and $h = 400$ nm. It is seen that the frequency of the relativistic plasma mode in a zero magnetic field remains practically unchanged in a wide range of parameter $2\pi\sigma_{2D}/c > 1$ values. However, when $2\pi\sigma_{2D}/c < 1$, the amplitude and frequency of the plasma mode begin to decrease sharply, and near $2\pi\sigma_{2D}/c \approx 0.3$ the mode vanishes (see the upper inset in Fig. 14). It is shown that a similar behavior of two-dimensional conductivity is demonstrated by the higher-frequency cyclotron mode [76].

Note that the condition $2\pi\sigma_{2D} > c$ for the excitation of relativistic plasma oscillations is much softer than the condition $\omega_p\tau \gg 1$ for the standard two-dimensional plasma excitations. The latter restricts the observation of plasma waves in present-day high-quality nanostructures to the range of cryogenic temperatures. For a typical mobility of up-to-

date GaAs-HEMT structures at room temperature, $\mu = 8000$ cm^2 (V s)$^{-1}$, the two-dimensional conductivity $2\pi\sigma_{2D}$ becomes greater than the velocity of light already at the concentration $n_s > 3 \times 10^{12}$ cm^{-2}. Thus, due to abnormally strong interaction with light, relativistic plasma excitations can be observed at temperatures up to room temperature. This fact is extremely attractive for various applications in plasmon electronics.

To illustrate, we carried out an experiment in the same microstructure geometry as in Fig. 13, but with an electron density of 4.4×10^{12} cm^{-2}. The measurements showed that for the studied disc at the excitation frequency $f = 1.3$ GHz the value of $2\pi\sigma_{2D}/c$ is 13.2 ($\omega\tau = 0.15$) at temperature $T = 4.2$ K and $2\pi\sigma_{2D}/c = 2.6$ ($\omega\tau = 0.017$) at $T = 300$ K. The lower inset in Fig. 14 shows the magnetoplasma relativistic resonance measured at $T = 4.2$, 160, and 300 K. The resonance is significantly broadened but is still observable even at a room temperature of 300 K, when $\omega\tau \ll 1$.

The physical nature of the discovered relativistic plasma mode is still not completely clear. However, the collection of experimental observations allows considering it a close relative of the new plasmon induced by metal proximity mentioned above [77, 78]. The main evidence of this analogy is that the relativistic plasmon arises only in the gated 2DES. Moreover, the frequency of both modes is a similar functional dependence on the dimensions of the gate and the distance from the gate to the quantum well.

6. Plasma excitations in two-dimensional materials

In recent times, interest in the investigation of plasma excitations in two-dimensional electron systems has significantly grown. Most early experiments were devoted to physical properties of plasma excitations in single-valley isotropic 2DESs based on MOS structures of AlGaAs/GaAs heterostructures [9, 13, 22]. During the last few decades, significant progress in epitaxial growth technology has led to the appearance of a new class of high-quality two-dimensional systems based on AlGaAs/AlAs and MgZnO/ZnO nanostructures.

Substantial drawbacks of AlGaAs/GaAs heterostructures include a small bandgap of 1.5 eV and, as a consequence, a low breakdown electric field and poor resistance to harsh environments. MgZnO/ZnO semiconductor heterostructures are free of these drawbacks. Their bandgap amounts to 3.4 eV which, in particular, enables using these structures as laser sources in the ultraviolet range. Moreover, ZnO-based structures are nontoxic and chemically stable. Therefore, MgZnO/ZnO heterostructures have promising potentialities for applications [88]. A distinctive feature of 2DESs based on AlAs quantum wells is the number of unique properties of the electron energy spectrum. The strong anisotropy of the effective masses of two-dimensional electrons and the controllable filling of different valleys make the heterostructures based on AlAs quantum wells a unique subject for studying new plasmonic phenomena [89].

Beginning in the 2000s, the development of nanotechnologies has been associated with a new two-dimensional material, graphene, which is a sheet of carbon atoms arranged in a hexagonal lattice. The main breakthrough in graphene production technology was the method of its micromechanical chipping from bulk graphite by means of adhesive tape [90, 91]. Graphene possesses a number of unique physical properties and is presently considered the most promising two-dimensional material. Sections 6.1–6.3 are devoted to comparing the physical properties of plasma excitations in various two-dimensional materials.

6.1 Plasma excitations of a two-dimensional electron system in MgZnO/ZnO nanostructures

Oxides, such as ZnO and its alloys, are one of the most promising types of new materials for the analysis of Coulomb correlations. Of primary interest are materials in which, by doping the ZnO oxide with magnesium Mg, it is possible to vary the bandgap width. Due to different spontaneous polarization in MgZnO and ZnO, it is possible to create a high-quality 2DES at their heterointerface. Over the past few years, it has been possible to obtain very high quality MgZnO/ZnO heterostructures. This is confirmed by the high mobility of two-dimensional electrons up to 8×10^5 cm^2 (V s)$^{-1}$ [92, 93]. ZnO-based low-dimensional systems are of particular interest, because the Coulomb interaction of two-dimensional electrons in such systems is much stronger than in low-dimensional structures based on GaAs semiconductor compounds. The significance of Coulomb correlations in two-dimensional systems is usually characterized by the dimensionless parameter r_s, defined as the ratio of Coulomb interaction energy E_C to Fermi energy E_F:

$$r_s = \frac{E_C}{E_F} = \frac{m^* e^2}{\varepsilon \hbar^2 \sqrt{\pi n_s}} \,. \tag{21}$$

Due to the large value of the electron effective mass in ZnO ($m^* \approx 0.29 m_0$) and the relatively small value of permittivity ($\varepsilon = 8.5$), the value of parameter r_s describing the Coulomb interaction in an electron system in ZnO-based structures appears to be almost an order of magnitude greater than in GaAs. In spite of the prospects of MgZnO/ZnO nanostructures for studies and applications, their energy band structure remains poorly studied. Microwave spectroscopy allowed the determination of the main conduction band parameters in the new two-dimensional electron system [94].

Figure 15a shows the magnetodispersion measured by the optical method in a 2DES sample of $Mg_xZn_{1-x}O/ZnO$ ($x = 0.02$) having the shape of a rectangle with the sides $a = 1.1$ mm and $b = 0.9$ mm [94]. The experiments were performed on a heterostructure with the density of two-dimensional electrons $n_s = 3.7 \times 10^{11}$ cm^{-2}. The inset in the figure shows the microwave absorption spectrum of the studied structure obtained in a zero magnetic field. From the spectrum, the resonance half-width is found to be $\Delta f = 5$ GHz, which corresponds to relaxation time $\tau = 30$ ps. To establish reliably the value of electron effective mass from the data presented in Fig. 15a, it should be noted that the upper cyclotron magnetoplasma mode can be described by the expression $\omega^2 = A + \omega_c^2$. Here, the constant A is the value of the shift caused by the plasma frequency, depending on the sample geometry. From the cyclotron frequency $\omega_c = eB/(m^* c)$, an unambiguous determination of the effective mass value is possible. The dependence of the electron effective mass in MgZnO/ZnO nanostructures on the two-dimensional concentration obtained in this way is shown in Fig. 15b. The dependence was obtained in six samples with different concentrations of two-dimensional electrons. The effective mass demonstrates substantial linear

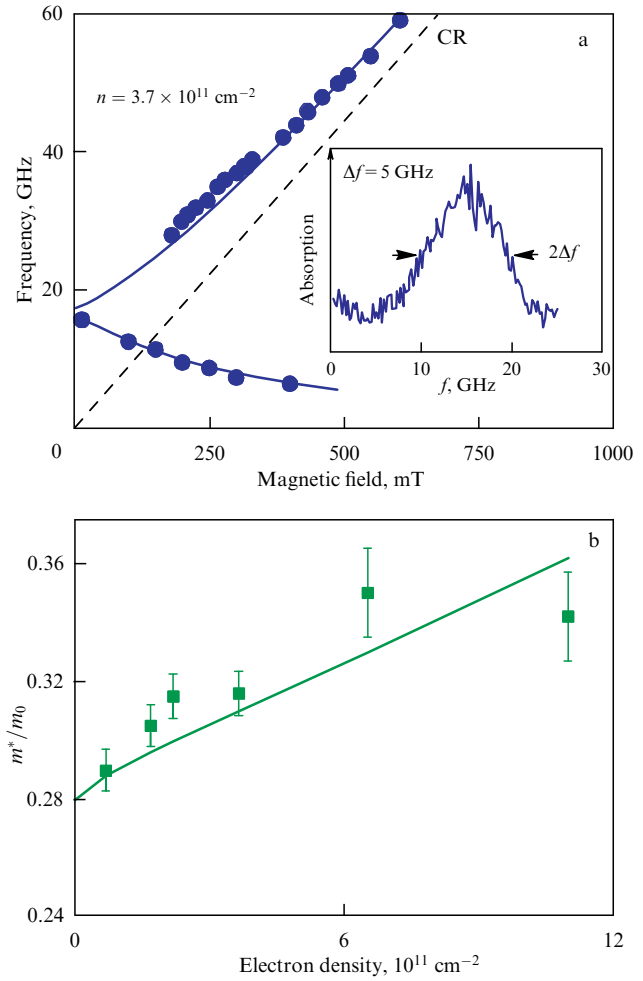

Figure 15. (a) Frequency of magnetoplasma resonances versus the magnitude of the perpendicular magnetic field in which the resonance occurs. The dashed line represents the cyclotron resonance $eB/(m^*c)$. The inset shows the absorption spectrum measured in a zero magnetic field. Half-width of the plasma resonance $\Delta f = 5$ GHz. (b) The dependence of the electron effective mass on the concentration obtained by the microwave spectroscopy method.

growth with an increase in the electron density. At present, this effect has no satisfactory explanation. Apparently, the observed increase in effective mass is related to the influence of Coulomb correlations under the conditions of Kohn theorem violation because of the conduction band nonparabolicity.

6.2 Plasma excitations of a two-dimensional electron system in AlGaAs/AlAs nanostructures

In recent decades, thanks to major progress in epitaxial growth technology, the appearance of high-quality two-dimensional structures of a new class based on AlAs quantum wells became possible [89]. Their distinctive features are the multi-valley structure and the natural anisotropy of the effective masses of two-dimensional electrons. Bulk AlAs is a nondirect band semiconductor that has three energy valleys in X points of the Brillouin zone. The Fermi surface of AlAs consists of three ellipsoids arranged along the principal crystallographic directions. In AlAs quantum wells more than 5 nm wide grown on GaAs (001) substrates, only the valleys X_x [100] and X_y [010] in the heterojunction plane are filled with electrons. This is due to biaxial compression of the AlAs

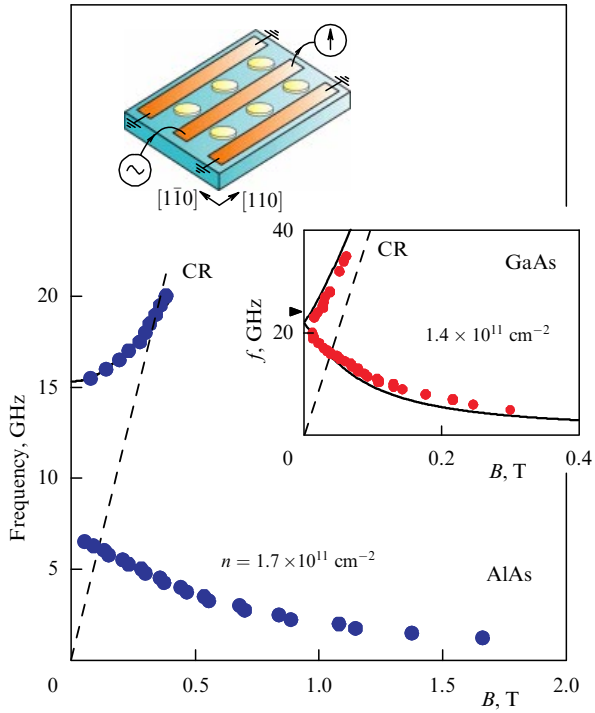

Figure 16. Magnetodispersion of plasma excitations in a disc with diameter $d = 0.5$ mm for electrons having an anisotropic energy spectrum in an AlAs quantum well. The dashed line shows the position of the cyclotron resonance. The upper part of the figure schematically depicts the studied sample. The inset presents the spectrum of magnetoplasma excitations measured in a geometrically identical sample with a GaAs quantum well with an isotropic effective mass of two-dimensional electrons.

layer, which arises due to the differences among the lattice constants in materials forming the heterojunction, namely, AlAs and AlGaAs. The effective mass values in the X_x and X_y valleys corresponding to the principal semiaxes of the ellipse are $m_l = 1.1\,m_0$ and $m_{tr} = 0.2\,m_0$.

The strong anisotropy of the effective masses of two-dimensional electrons and the controlled filling of valleys make 2D structures based on AlAs quantum wells a unique subject for studying new plasmonic phenomena. The first experiments with AlAs heterostructures showed that the magnetoplasma excitation spectrum in such systems has a number of unique properties: the presence of a gap in the spectrum of plasma excitations in perfectly symmetric disc-shaped samples, as well as the nontrivial transformation of the plasmon spectrum when there is a redistribution of charge carriers between different valleys [95–98].

Measurements of plasma excitation dispersion for electrons with an anisotropic energy spectrum were performed using the coplanar technique [95]. In these measurements, the sample consisted of six equidistant 2DES discs, $d = 0.5$ mm in diameter, placed in the gap of a matched microwave coplanar waveguide (Fig. 16). The transmission of a microwave signal through the coplanar waveguide was measured. The experiments were performed using 2DESs based on an AlAs quantum well grown by molecular beam epitaxy on an undoped GaAs substrate along the [100] crystallographic direction. The quantum well width amounted to 15 nm, the electron concentration n_s and mobility μ being 1.7×10^{11} cm^{-2} and 2.0×10^5 cm^2 (V s)$^{-1}$, respectively.

The magnetodispersion dependence obtained in these experiments is presented in Fig. 16. The magnetodispersion

has two branches separated by a gap in a zero magnetic field. The low-frequency branch having negative magnetodispersion corresponds to the excitation of an edge magnetoplasmon [22, 28], whereas the high-frequency branch, whose magnetodispersion is positive, corresponds to the excitation of a cyclotron magnetoplasmon mode. In single-valley isotropic systems based on GaAs ($m^* = 0.067m_0$), the cyclotron and edge magnetoplasma modes are degenerate in a zero magnetic field (see the inset in Fig. 16). The anisotropy of electron masses in AlAs leads to the removal of this degeneracy and the appearance of a gap in the spectrum (see Fig. 16). This observation seems particularly surprising, if we take into account that the degeneracy removal occurs in a zero magnetic field under perfect symmetry of the disc geometry [99]. A similar phenomenon was observed in AlGaAs/GaAs heterostructures [100, 101], where a minor anisotropy was induced by a strong magnetic field in the sample plane.

Electric field **E** oriented along the crystallographic direction $[1\bar{1}0]$ can be presented as a sum of two components along two principal directions, [100] and [010]: $\mathbf{E} = \mathbf{E}_{\rm l} + \mathbf{E}_{\rm tr}$. In a zero magnetic field, $B = 0$, each of these components excites its own plasma wave with the corresponding effective mass $m_{\rm l}$ or $m_{\rm tr}$. The frequencies $\Omega_{\rm l,\,tr}$ of these plasma waves are determined by the standard expression [7]

$$\Omega^2_{\rm l,\,tr} = \frac{n_{\rm s} e^2}{2 m_{\rm l,\,tr} \varepsilon_0 \varepsilon}\, q\,, \tag{22}$$

where $\varepsilon = (\varepsilon_{\rm GaAs} + 1)/2$ is the effective permittivity of the surrounding medium, and $q = 2.4/d$ is the wave vector for the disc geometry [13]. Using Eqn (22) and the experimental values for the plasma frequencies $\Omega_{\rm l} = 6.5$ GHz and $\Omega_{\rm tr} = 15.3$ GHz, the following values of effective masses in AlAs quantum wells can be obtained: $m_{\rm l} = (1.10 \pm 0.05)m_0$, $m_{\rm tr} = (0.20 \pm 0.01)m_0$. It is worth noting that this is the first direct experimental determination of charge carrier effective masses in semiconductor AlAs nanostructures. The obtained values of effective masses are in perfect agreement with literature data [102–104].

One of the most remarkable physical properties of 2DESs based on AlAs quantum wells is the possibility of controlling the filling of different X-valleys. The control can be implemented by either a uniaxial deformation [105] or quantum confinement [106, 107]. This property makes semiconductor AlAs nanostructures a promising material for new valleytronic elements — electronic devices using the degree of freedom related to the energy valley of an electron rather than its charge.

Let us dwell on the possibility of controlling the valley degree of freedom by quantum confinement. In wide AlAs quantum wells ($W > 5.5$ nm) grown on a GaAs (001) substrate, electrons fill the values X_x [100] and X_y [010] in the plane of the quantum well. Each of these valleys has a strongly anisotropic Fermi contour. This seems somewhat strange, because the dimensional quantization is expected to facilitate the X_z valley being the lowest-energy one (since its effective mass in the direction perpendicular to the quantum well plane is greater). However, the biaxial compression arising due to the difference between the AlAs and AlGaAs lattice constants appeared to cause an inversion of valleys [106, 107]. In narrow AlAs quantum wells ($W < 5.5$ nm), electrons begin to fill the X_z [001] valley, which is isotropic in the quantum well plane. The first experiments on studying the

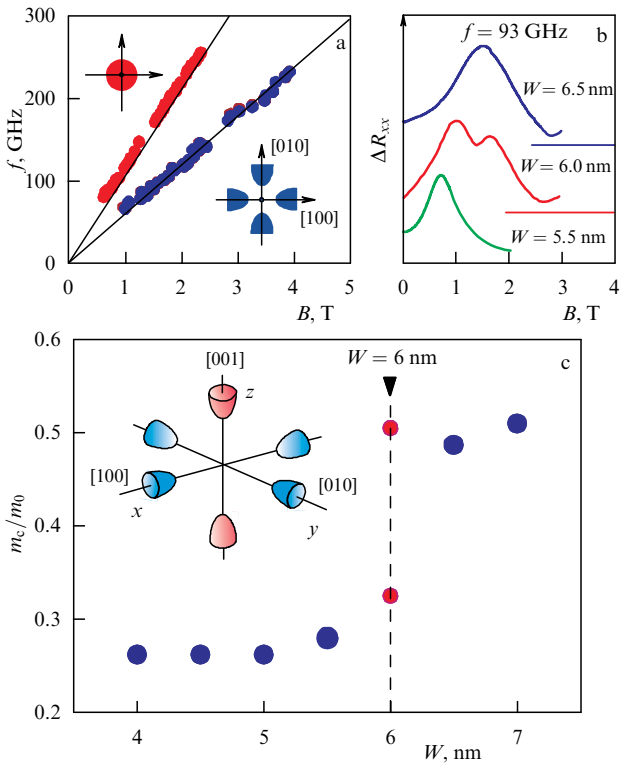

Figure 17. (Color online.) (a) 2D magnetoplasmon magnetodispersions measured in AlAs quantum wells with width $W = 5.5$ nm (red dots) and $W = 6.5$ nm (blue dots). The solid lines correspond to the cyclotron resonance. The insets schematically show the two-dimensional Fermi contours for filling the valleys X_z and $X_x - X_y$. (b) Magnetic field dependences of microwave radiation-induced changes in longitudinal magnetoresistance ΔR_{xx} obtained for AlAs quantum wells with different widths: $W = 5.5$ nm (green curve), $W = 6.0$ nm (red curve), and $W = 6.5$ nm (blue curve). All dependences are measured for the same frequency of irradiation, 93 GHz. (c) Experimental dependence of the cyclotron effective mass on the AlAs quantum well width. The dashed line marks data corresponding to borderline width $W = 6$ nm, at which the $\Gamma - X$ transition in the filling of valleys occurs.

energy $\Gamma - X$ transition in AlAs narrow quantum wells were implemented by the indirect transport method using the temperature dependences of Shubnikov–de Haas oscillations [107–110].

The most direct and accurate method of studying Fermi surfaces in semiconductors is microwave magnetospectroscopy [19]. This method was applied by the authors of the present review to the detailed analysis of the $\Gamma - X$ intervalley transition, as well as plasma dynamics in narrow AlAs quantum wells [97, 98]. The measurements were carried out using the double synchronous technique of microwave absorption transport detection [111]. The studied samples were prepared from AlAs/$Al_xGa_{1-x}As$ ($x = 0.46$) heterostructures with the quantum well width $W = 4.0$, 4.5, 5.0, 5.5, 6.0, 6.5, 7.0, and 15 nm. The samples had the shape of Hall bridges with width $L = 100$ μm and the distance between the nearest contacts of 1.0 mm (Fig. 17). A typical value of the electron density for the studied structures was $n_{\rm s} = 4.6 \times 10^{11}$ cm^{-2}.

Figure 17a shows the magnetodispersion of plasma excitations measured for two structures with identical geometries but different widths of quantum wells, $W =$ 5.5 nm and 6.5 nm. The resonance strictly follows the cyclotron resonance line $f_{\rm c} = \omega_{\rm c}/(2\pi) = eB/(2\pi m_{\rm c} c)$, where

m_c is the effective cyclotron mass of the electron, $m_c(W = 5.5\ \text{nm}) = (0.28 \pm 0.01)\, m_0$ and $m_c(W = 6.5\ \text{nm}) = (0.49 \pm 0.01)\, m_0$. To clarify what happens, let us consider the situation when both valleys, X_x and X_y, in the quantum well plane are filled. The Fermi contour in this case is an ellipse with two effective masses along the principal crystallographic axes $m_l = 1.1\, m_0$ and $m_{tr} = 0.2\, m_0$. Then, the cyclotron mass of two-dimensional electrons is determined by the geometric mean value of $m_c = \sqrt{m_l m_{tr}} = 0.47\, m_0$. If the electrons fill the valley X_z located out of the quantum well plane, the Fermi contour is merely a circle. Therefore, the cyclotron mass coincides with the effective mass of charge carriers, $m_c = m_{tr} = 0.2\, m_0$. The effective mass value obtained in the experiment for the AlAs quantum well with width $W = 6.5$ nm means that in the structure the planar anisotropic valleys $X_x - X_y$ are filled. The measured value of the cyclotron mass of electrons in the quantum well with $W = 5.5$ nm shows that the isotropic X_z valley is filled in it. Thus, between these two cases, a unique $\Gamma - X$ transition in the energy spectrum of two-dimensional electrons in narrow AlAs quantum wells is observed.

Figure 17b presents the photoresponse curves measured at the frequency $f = 93$ GHz for three structures with quantum well width $W = 6.5$ nm (blue), $W = 6.0$ nm (red), and $W = 5.5$ nm (green). A change in the quantum well width severely affects the observed position and shape of the cyclotron magnetoplasma resonance. For quantum wells with width $W = 5.5$ nm and 6.5 nm, a single resonance is observed arising in different magnetic fields. As shown above, in these structures the electrons occupy two different energy valleys. For the quantum well with width $W = 6.0$ nm, two resonances are observed at a time. Thus, a unique transient situation occurs when a balance in filling the X_z and X_{x-y} valleys is achieved. In this case, it is possible to controllably switch the filling of X_z and X_{x-y} valleys by applying external pressure or an electric field. To switch the filling of different valleys is the main operation needed for functioning of valleytronic devices.

Figure 17c shows the resulting dependence of cyclotron mass of two-dimensional electrons in a quantum AlAs well. The dashed line in Fig. 17c marks the data for the transient quantum well with $W = 6$ nm, where the switching of valleys occurs. Note that the experimentally obtained value of the cyclotron effective mass of electrons in the X_z valley $m_c(W = 5.5\ \text{nm}) = (0.28 \pm 0.01)\, m_0$ substantially exceeds the band effective mass of the bulk AlAs $m^* = 0.2\, m_0$ [112]. Additional experiments have excluded nonparabolicity and retardation effects as possible reasons for the mass increase. This controversy requires further study.

6.3 Plasma excitations in graphene

The system of two-dimensional electrons in graphene attracts significant interest due to its unusual physical properties — the linear massless dispersion law corresponding to the Dirac relativistic spectrum and the absence of an energy gap [90, 91],

$$E(k) = \hbar v_0 k\,, \tag{23}$$

where $v_0 \approx 10^6$ m s^{-1} is a single-particle velocity of charge carriers in graphene. Therefore, the Fermi energy is expressed as $E_F = \hbar v_0 \sqrt{n_s}$.

However, the overwhelming majority of results obtained for 2DESs in graphene are explained within a single-particle picture, while collective effects are barely manifested in graphene. First, this is due to the high Fermi energy (because of the linear dispersion law), as well as to the considerable amplitude of the random potential that inevitably arises in a single-layered structure. One of the most evident manifestations of collective properties in an electron system is the plasma oscillations. In graphene, the plasma frequency is determined by the expression [113]

$$\omega_p^2 = \frac{2\pi n_s e^2}{m^* \varepsilon}\, q = \frac{2 v_0 e^2}{\hbar\, \varepsilon}\, \sqrt{\pi n_s}\, q\,. \tag{24}$$

Here, we used the following expression for the electron effective mass:

$$m^* = \frac{\hbar^2}{2\pi}\left(\frac{\partial A}{\partial E}\right) = \frac{\hbar}{v_0}\, \sqrt{\pi n_s}\,, \tag{25}$$

where $A = \pi k^2$ is the area of the Fermi surface in the k-space.

The first experimental studies on plasma excitations in graphene confirmed the standard dispersion law (24). These experiments were performed in arrays of strips and discs using infrared (IR) spectroscopy [114, 115]. Subsequent experimental investigations of collective excitations in graphene became possible using the innovative technique of near-field IR nanoscopy and microscopy [116, 117]. However, the first measurements have shown that the characteristic resonance width exceeds 10 meV, which is a thousand times greater than the typical width of analogous resonances measured in AlGaAs/GaAs nanostructures. Thus, the system of two-dimensional electrons in graphene is characterized by very high inhomogeneity and disorder, which leads to abnormally great broadening of resonance absorption lines and limits the capabilities of plasma wave investigation.

Inelastic light scattering is one of the methods used to study collective excitations in graphene [118]. Figure 18a presents the spectrum of inelastic scattering of light, obtained in different magnetic fields directed perpendicular to the graphene plane. The measurements were carried out on a superhigh-quality sample of free-standing graphene with the characteristic size of 10 μm. At a concentration of 2×10^{11} cm^{-2}, the electron transport mobility amounted to 2×10^5 cm^2 (V s)$^{-1}$. Figure 18a shows that, as the magnetic field increases, the line of inelastic light scattering shifts towards higher energies. The dependence of the Raman shift of this line on the magnetic field is presented in Fig. 18b. The figure shows that the magnetic field dependence of the spectral shift corresponds to the standard dependence, which is observed for cyclotron magnetoplasma excitations and is associated with the hybridization of plasma and cyclotron energies. Although the electron dispersion in graphene is linear rather than quadratic, at high filling factors (in the quasiclassical limit) the Landau levels appear practically equidistant, and the standard law of mode hybridization $\omega^2 = \omega_p^2 + \omega_c^2$ is valid. Indeed, in Fig. 18c, the dependence $E^2 = (\hbar\omega)^2$ on B^2 is shown. The quadratic law describes well the mode hybridization within the entire range of magnetic field values.

Figure 19a shows the dependence of electron cyclotron energy on the magnetic field in free-standing graphene determined from the magnetoplasma line spectral shift under a concentration of 3×10^{11} cm^{-2} and $T = 1.5$ K. It is seen that, in accordance with Eqn (19), this dependence is a linear function of magnetic field, and from the slope of this dependence with Eqn (25) taken into account it is possible to

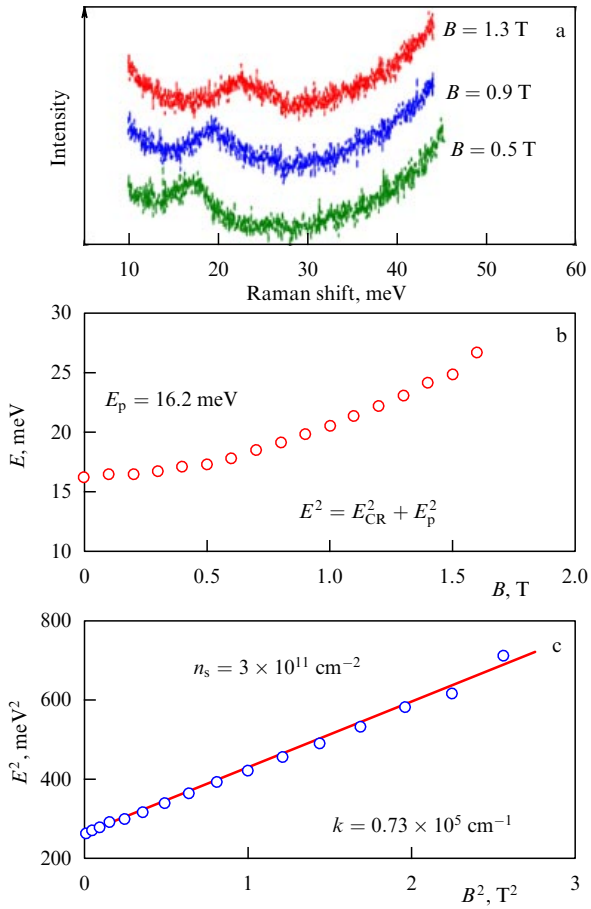

Figure 18. (a) Spectrum of inelastic light scattering measured at different magnitudes of a magnetic field in free-standing graphene. The curves demonstrate well-distinguishable magnetoplasmon resonance. (b) The magnetoplasmon line Raman shift dependence on the magnetic field. (c) The same dependence presented in the squared energy–squared magnetic field coordinates.

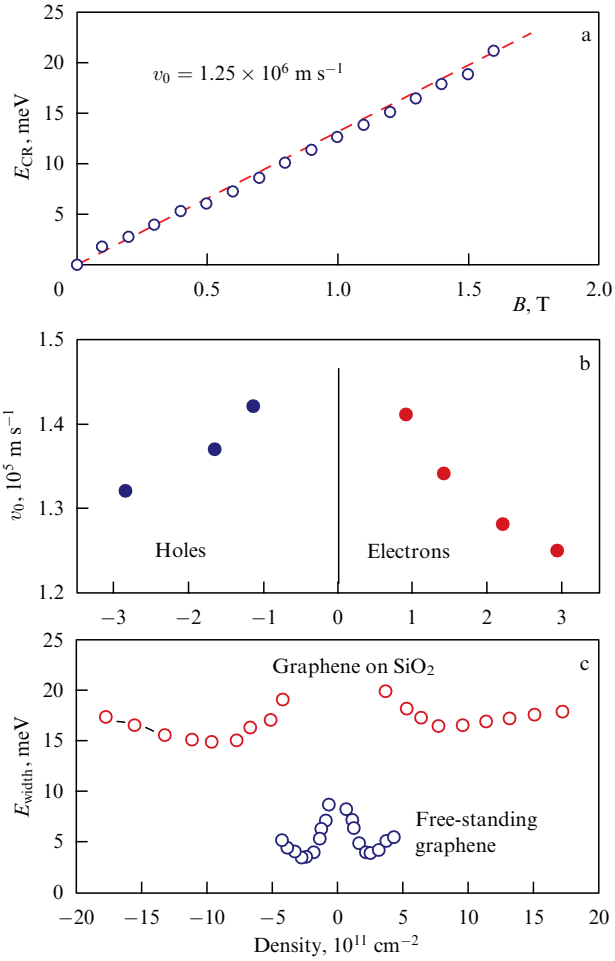

Figure 19. (a) Magnetic field dependence of the cyclotron energy of electrons in free-standing graphene, found from the spectral shift of the magnetoplasma line at a concentration of 3×10^{11} cm^{-2}. (b) The dependences of the velocity of electrons and holes in free-standing graphene on their concentration. (c) The dependences of magnetoplasma line width on the concentration of electrons and holes, measured in graphene lying on silicon dioxide and free graphene hanging on contacts.

extract the velocity of charge carriers at different densities,

$$E_{CR} = \hbar\omega_c = \frac{ev_0}{c\sqrt{\pi n_s}}\, B\,. \tag{26}$$

At an electron concentration of 3×10^{11} cm^{-2}, the velocity of electrons in free-standing graphene appeared to be $v_0 = 1.25 \times 10^6$ m s^{-1}, which is somewhat higher than the generally accepted value of 1.05×10^6 m s^{-1}. It appears that, as the density of electrons and holes decreases, their velocity does not remain constant, but considerably increases. From Fig. 19b, it is seen that at an electron concentration of about 10^{11} cm^{-2}, the velocity of both electrons and holes increases to 1.43×10^6 m s^{-1}, which exceeds the standard value by almost 40%. The increase in velocity of electrons and holes at low concentrations means that the dispersion of charge carriers in graphene at small momenta becomes sublinear, which is most likely due to interaction effects that lead to renormalization of dispersion [119, 120].

The resonance line width is one of the most important parameters of plasma oscillations. It directly determines the quality of a structure and the relaxation time of charge carriers $\Delta\omega = 1/\tau$. Figure 19c presents the dependences of line width of plasma excitations on the concentration, measured by the inelastic light scattering method in graphene. For comparison, the figure shows the dependences measured in graphene lying on a silicon dioxide substrate and in free-standing graphene. First, line broadening in the free-standing graphene is seen to be almost five times smaller than in the graphene on an SiO_2 substrate, which evidences much higher perfection of the electron system realized in the former case. Moreover, the resonance in the free-standing graphene attains its minimal width of 3.5 meV at the concentration of electrons and holes of about 2.5×10^{11} cm^{-2}, whereas in the graphene on the substrate its minimal line width of 14.8 meV is observed at much higher densities of 6.5×10^{11} cm^{-2}. An important result is that in the free-standing graphene at concentrations below 2×10^{11} cm^{-2} the resonance lines begin to broaden sharply, which evidences the increasing inhomogeneity in the electron system and the appearance of separate domains with different densities of electrons and holes. The inhomogeneity in concentration manifests itself in the spatial fluctuations of plasma frequency, which naturally leads to the broadening of the magnetoplasma line.

To conclude this section, we summarized in the table the main physical parameters characterizing the properties of plasma excitations in various two-dimensional materials. We should note that due to the massless nature of electrons in graphene the high mobility of charge carriers in graphene

Table. Characteristics of plasma excitations in two-dimensional materials.

Material	Carrier mass	Relaxation time, ps	References
AlGaAs/GaAs nanostructures	$0.067\,m_0$	160	[11]
AlGaAs/AlAs nanostructures	$m_{\rm tr} = 0.2\,m_0$, $m_{\rm l} = 1.1\,m_0$	50	[95]
MgZnO/ZnO nanostructures	$(0.3-0.35)\,m_0$	30	[94]
Graphene	$(0-0.07)\,m_0$	1.6	[91, 121, 122]

cannot serve as an indicator of 2DES high quality. A specific feature of graphene is that, when the carrier density decreases (to zero), the conductivity of the system remains finite, while the carrier mass according to Eqn (25) tends to zero. Therefore, it looks as if the mobility of electrons and holes becomes infinity. Naturally, such a conclusion is wrong, and the explanation is that in the low-concentration limit the system becomes inhomogeneous, i.e., divides into domains consisting of electrons and holes, so that the charge carrier concentration never becomes zero. Therefore, at low concentrations, it is impossible to determine the mobility of electrons and holes. Thus, a real parameter reflecting the purity of structures is the relaxation time of charge carriers or the plasma resonance line width.

7. Conclusion

The study of two-dimensional electron systems is one of the most relevant and rapidly progressing fields of solid-state physics. Two-dimensional electron systems are mainly interesting because many physical phenomena observed in them have direct analogs in the three-dimensional world. While most three-dimensional many-particle problems have no analytical solution, in the two-dimensional case, we can often manage to find a solution to such problems. On the other hand, one-dimensional systems are too trivial from a theoretical point of view and far from the real world.

For the physics of two-dimensional electron systems, a key issue is the study of properties of their collective excitations. One of the most important representatives of the class of collective excitation is a wave of charge density — the plasmon. The response of a 2DES to an electromagnetic wave in a wide range of practically significant frequencies is exclusively due to the collective plasma motion of all electrons of the system. This is because the velocity of two-dimensional plasma waves significantly exceeds the Fermi velocity of individual electrons in 2DESs. In contrast to the velocity of plasma waves in three-dimensional materials, e.g., metals, the velocity of two-dimensional plasmons is easily varied by changing the electron concentration or by applying an external magnetic field.

All the above properties make the plasma waves in two-dimensional electron systems a flexible and convenient tool for physical studies in many different fields. No doubt, this area of physics will delight us for a long time with its new, sometimes unpredictable, surprises. We can also assume with a high degree of confidence that in the near future the next page will be turned, related to plasmon polaritons and their numerous applications in the microwave and terahertz spectral regions.

This study was supported by the Russian Science Foundation (grant no. 19-72-30003).

References

1. Landau L *Phys. Rev.* **60** 356 (1941)
2. Bohm D, Pines D *Phys. Rev.* **82** 625 (1951)
3. Pines D, Bohm D *Phys. Rev.* **85** 338 (1952)
4. Bohm D, Pines D *Phys. Rev.* **92** 609 (1953)
5. Pines D *Rev. Mod. Phys.* **28** 184 (1956)
6. Tonks L, Langmur I *Phys. Rev.* **33** 195 (1929)
7. Stern F *Phys. Rev. Lett.* **18** 546 (1967)
8. Grimes C C, Adams G *Phys. Rev. Lett.* **36** 145 (1976)
9. Allen S J (Jr) et al. *Phys. Rev. Lett.* **38** 980 (1977)
10. Theis T N, Kotthaus J P, Stiles P J *Solid State Commun.* **24** 273 (1977)
11. Andreev I V et al. *Appl. Phys. Lett.* **105** 202106 (2014)
12. Zhang Q et al. *Phys. Rev. Lett.* **113** 047601 (2014)
13. Kukushkin I V et al. *Phys. Rev. Lett.* **90** 156801 (2003)
14. Kukushkin I V et al. *JETP Lett.* **77** 497 (2003); *Pis'ma Zh. Eksp. Teor. Fiz.* **77** 594 (2003)
15. Kukushkin I V et al. *Phys. Rev. B* **73** 113310 (2006)
16. Gusikhin P A et al. *Phys. Rev. Lett.* **121** 176804 (2018)
17. Chaplik A V *Surface Sci. Rep.* **5** 289 (1985)
18. Dorfman Ya G *Dokl. Akad. Nauk SSSR* **81** 765 (1951)
19. Dresselhaus G, Kip A F, Kittel C *Phys. Rev.* **98** 368 (1955)
20. Chaplik A V *Sov. Phys. JETP* **35** 395 (1972); *Zh. Eksp. Teor. Fiz.* **62** 746 (1972)
21. Chiu K W, Quinn J J *Phys. Rev. B* **9** 4724 (1974)
22. Allen S J (Jr) et al. *Phys. Rev. B* **28** 4875(R) (1983)
23. Glattli D C et al. *Phys. Rev. Lett.* **54** 1710 (1985)
24. Mast D B, Dahm A J, Fetter A L *Phys. Rev. Lett.* **54** 1706 (1985)
25. Govorkov S A et al. *JETP Lett.* **17** 487 (1986); *Pis'ma Zh. Eksp. Teor. Fiz.* **44** 380 (1986)
26. Muravev V M et al. *Phys. Rev. Lett.* **101** 216801 (2008)
27. Peters P J M et al. *Phys. Rev. Lett.* **67** 2199 (1991)
28. Volkov V A, Mikhailov S A *Sov. Phys. JETP* **67** 1639 (1988); *Zh. Eksp. Teor. Fiz.* **94** 217 (1988)
29. Volkov V A et al. *JETP Lett.* **44** 655 (1986); *Pis'ma Zh. Eksp. Teor. Fiz.* **44** 510 (1986)
30. Talyanskii V I et al. *Phys. Rev. B* **46** 12427 (1992)
31. Zhitenev N B et al. *Phys. Rev. Lett.* **71** 2292 (1993)
32. Khannanov M N, Fortunatov A A, Kukushkin I V *JETP Lett.* **93** 657 (2011); *Pis'ma Zh. Eksp. Teor. Fiz.* **93** 736 (2011)
33. Andreev I V et al. *Phys. Rev. B* **86** 125315 (2012)
34. Andreev I V, Murav'ev V M, Kukushkin I V *JETP Lett.* **96** 536 (2012); *Pis'ma Zh. Eksp. Teor. Fiz.* **96** 588 (2012)
35. Ashkinadze B M et al. *Phys. Status Solidi A* **164** 231 (1997)
36. Kukushkin I V et al. *Nature* **415** 409 (2002)
37. Fetter A L *Phys. Rev. B* **33** 5221 (1986)
38. Zagitova A A et al. *JETP Lett.* **108** 446 (2018); *Pis'ma Zh. Eksp. Teor. Fiz.* **108** 478 (2018)
39. Shikin V et al. *Phys. Rev. B* **43** 11903 (1991)
40. Muravev V M et al. *Phys. Rev. B* **96** 045421 (2017)
41. Muravev V M et al. *JETP Lett.* **109** 663 (2019); *Pis'ma Zh. Eksp. Teor. Fiz.* **109** 685 (2019)
42. Sommerfeld A *Ann. Physik* **303** 233 (1899)
43. Das Sarma S, Lai W *Phys. Rev. B* **32** 1401(R) (1985)
44. Eliasson G et al. *Solid State Commun.* **60** 41 (1986)
45. Aleiner I L, Yue D, Glazman L I *Phys. Rev. B* **51** 13467 (1995)
46. Koval'skii V A et al. *JETP Lett.* **84** 560 (2006); *Pis'ma Zh. Eksp. Teor. Fiz.* **84** 656 (2006)
47. Demel T et al. *Phys. Rev. Lett.* **66** 2657 (1991)
48. Goñi A R et al. *Phys. Rev. Lett.* **67** 3298 (1991)
49. Kukushkin I V et al. *Phys. Rev. B* **72** 161317(R) (2005)
50. Burke P J et al. *Appl. Phys. Lett.* **76** 745 (2000)
51. Kulik L V, Kirpichev V E *Phys. Usp.* **49** 353 (2006); *Usp. Fiz. Nauk* **176** 365 (2006)
52. Muravev V M et al. *Phys. Rev. B* **75** 193307 (2007)
53. Andress W F et al. *Nano Lett.* **12** 2272 (2012)
54. Yeung K Y M et al. *Appl. Phys. Lett.* **102** 021104 (2013)
55. Gubarev S I et al. *JETP Lett.* **102** 461 (2015); *Pis'ma Zh. Eksp. Teor. Fiz.* **102** 517 (2015)
56. Iranzo D A et al. *Science* **360** 291 (2018)
57. Ryzhii V et al. *J. Appl. Phys.* **96** 7625 (2004)
58. Satou A, Ryzhii V, Chaplik A *J. Appl. Phys.* **98** 034502 (2005)

59. Mikhailov S A, Savostianova N A *Phys. Rev. B* **74** 045325 (2006)
60. Popov V V, Polishchuk O V, Nikitov S A *JETP Lett.* **95** 85 (2012); *Pis'ma Zh. Eksp. Teor. Fiz.* **95** 91 (2012)
61. Gubarev S I et al. *JETP Lett.* **90** 539 (2009); *Pis'ma Zh. Eksp. Teor. Fiz.* **90** 588 (2009)
62. Mikhailov S A *Phys. Rev. B* **70** 165311 (2004)
63. Mikhailov S A, Savostianova N A *Phys. Rev. B* **71** 035320 (2005)
64. Chiu K W, Lee T K, Quinn J J *Surf. Sci.* **58** 182 (1976)
65. Mikhailov S A *Phys. Rev. B* **54** 10335 (1996)
66. Andreev I V et al. *JETP Lett.* **102** 821 (2015); *Pis'ma Zh. Eksp. Teor. Fiz.* **102** 938 (2015)
67. Muravev V M et al. *Phys. Rev. B* **93** 041110(R) (2016)
68. Fal'ko V I, Khmel'nitskii D E *Sov. Phys. JETP* **68** 1150 (1989); *Zh. Eksp. Teor. Fiz.* **95** 1988 (1989)
69. Purcell E M *Phys. Rev.* **69** 681 (1946)
70. Muravev V M et al. *Phys. Rev. B* **83** 075309 (2011)
71. Scalari G et al. *Science* **335** 1323 (2012)
72. Forn-Díaz P et al. *Rev. Mod. Phys.* **91** 025005 (2019)
73. Dicke R H *Phys. Rev.* **93** 99 (1954)
74. Gusikhin P A, Murav'ev V M, Kukushkin I V *JETP Lett.* **100** 648 (2014); *Pis'ma Zh. Eksp. Teor. Fiz.* **100** 732 (2014)
75. Muravev V M et al. *Phys. Rev. Lett.* **114** 106805 (2015)
76. Gusikhin P A, Muravev V M, Kukushkin I V *JETP Lett.* **102** 749 (2015); *Pis'ma Zh. Eksp. Teor. Fiz.* **102** 859 (2015)
77. Muravev V M et al. *Phys. Rev. B* **99** 241406(R) (2019)
78. Zabolotnykh A A, Volkov V A *Phys. Rev. B* **99** 165304 (2019)
79. Muravev V M et al. *Phys. Rev. B* **100** 205405 (2019)
80. Zarezin A M et al. *JETP Lett.* **111** 282 (2020); *Pis'ma Zh. Eksp. Teor. Fiz.* **111** 316 (2020)
81. Mackens U et al. *Phys. Rev. Lett.* **53** 1485 (1984)
82. Demel T et al. *Phys. Rev. Lett.* **66** 2657 (1991)
83. Dyakonov M I, Shur M S *IEEE Trans. Electron Devices* **43** 1640 (1996)
84. Shur M S, Ryzhii V *Int. J. High Speed Electron. Syst.* **13** 575 (2003)
85. Knap W et al. *J. Infrared Milli. Terahz Waves* **30** 1319 (2009)
86. Muravev V M, Kukushkin I V *Appl. Phys. Lett.* **100** 082102 (2012)
87. Muravev V M et al. *JETP Lett.* **103** 380 (2016); *Pis'ma Zh. Eksp. Teor. Fiz.* **103** 428 (2016)
88. Schmidt-Mende L, MacManus-Driscoll J L *Mater. Today* **10** (5) 40 (2007)
89. Shayegan M et al. *Phys. Status Solidi B* **243** 3629 (2006)
90. Novoselov K S et al. *Science* **306** 666 (2004)
91. Novoselov K S et al. *Nature* **438** 197 (2005)
92. Falson J et al. *Appl. Phys. Express* **4** 091101 (2011)
93. Maryenko D et al. *Phys. Rev. Lett.* **108** 186803 (2012)
94. Kozlov V E et al. *Phys. Rev. B* **91** 085304 (2015)
95. Muravev V M et al. *Phys. Rev. B* **92** 041303(R) (2015)
96. Khisameeva A R et al. *JETP Lett.* **106** 26 (2017); *Pis'ma Zh. Eksp. Teor. Fiz.* **106** 29 (2017)
97. Khisameeva A R et al. *Phys. Rev. B* **97** 115308 (2018)
98. Khisameeva A R et al. *J. Appl. Phys.* **125** 154501 (2019)
99. Dahl C et al. *Solid State Commun.* **80** 673 (1991)
100. Kozlov V E, Gubarev S I, Kukushkin I V *JETP Lett.* **94** 397 (2011); *Pis'ma Zh. Eksp. Teor. Fiz.* **94** 429 (2011)
101. Kozlov V E et al. *JETP Lett.* **96** 525 (2012); *Pis'ma Zh. Eksp. Teor. Fiz.* **96** 576 (2012)
102. Miura N et al. *Solid State Commun.* **79** 1039 (1991)
103. Lay T S et al. *Appl. Phys. Lett.* **62** 3120 (1993)
104. Gunawan O et al. *Phys. Rev. Lett.* **93** 246603 (2004)
105. Gunawan O et al. *Phys. Rev. Lett.* **97** 186404 (2006)
106. van Kesteren H W et al. *Phys. Rev. B* **39** 13426 (1989)
107. Yamada S et al. *Phys. Rev. B* **49** 2189 (1994)
108. van de Stadt A F W et al. *Surf. Sci.* **361–362** 521 (1996)
109. Vakili K et al. *Phys. Rev. Lett.* **92** 226401 (2004)
110. Gokmen T et al. *Phys. Rev. B* **79** 195311 (2009)
111. Vasiliadou E et al. *Phys. Rev. B* **48** 17145 (1993)
112. Adachi S *J. Appl. Phys.* **58** R1 (1985)
113. Lozovik Yu E, Merkulova A A, Sokolik A A *Phys. Usp.* **51** 727 (2008); *Usp. Fiz. Nauk* **178** 757 (2008)
114. Yan H et al. *Nat. Nanotechnol.* **7** 330 (2012)
115. Yan H et al. *Nano Lett.* **12** 3766 (2012)
116. Chen J et al. *Nature* **487** 77 (2012)
117. Fei Z et al. *Nature* **487** 82 (2012)
118. Kukushkin V I, Kirpichev V E, Kukushkin I V *JETP Lett.* **104** 37 (2016); *Pis'ma Zh. Eksp. Teor. Fiz.* **104** 32 (2016)
119. Das Sarma S, Hwang E H, Tse W-K *Phys. Rev. B* **75** 121406(R) (2007)
120. Levitov L S, Shtyk A V, Feigelman M V *Phys. Rev. B* **88** 235403 (2013)
121. Yoon H et al. *Nat. Nanotechnol.* **9** 594 (2014)
122. Ni G X et al. *Nature* **557** 530 (2018)